Hydroelastic response of an ice sheet with a lead to a moving load

Y. Z. Xue (薛彦卓), [iD] L. D. Zeng (曾令东), [iD] B. Y. Ni (倪宝玉), [iD] A. A. Korobkin, and [iD] T. I. Khabakhpasheva

View Online   Export Citation   CrossMark

ARTICLES YOU MAY BE INTERESTED IN

An improved higher-order moving particle semi-implicit method for simulations of two-dimensional hydroelastic slamming
Physics of Fluids **33**, 037104 (2021); https://doi.org/10.1063/5.0033491

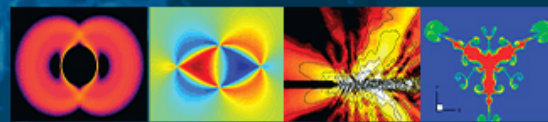Numerical validation and physical explanation of the universal force theory of three-dimensional steady viscous and compressible flow
Physics of Fluids **33**, 036107 (2021); https://doi.org/10.1063/5.0039243

Aerodynamic interaction of bristled wing pairs in fling
Physics of Fluids **33**, 031901 (2021); https://doi.org/10.1063/5.0036018

Physics of Fluids
GALLERY OF COVERS

Hydroelastic response of an ice sheet with a lead to a moving load

Y. Z. Xue (薛彦卓),[1] L. D. Zeng (曾令东),[1] B. Y. Ni (倪宝玉),[1,a] A. A. Korobkin,[2,3] and T. I. Khabakhpasheva[2,3]

AFFILIATIONS

[1]College of Shipbuilding Engineering, Harbin Engineering University, Harbin 150001, People's Republic of China
[2]School of Mathematics, University of East Anglia, Norwich NR4 7TJ, United Kingdom
[3]Lavrentyev Institute of Hydrodynamics, pr. Lavrentyeva 15, Novosibirsk 630090, Russia

[a]Author to whom correspondence should be addressed: nibaoyu@hrbeu.edu.cn

ABSTRACT

The hydroelastic symmetric response of a floating ice sheet caused by a pressure moving either in the ice lead or on the infinite ice sheet with a crack (a lead of zero width) is investigated. The ice sheet is modeled as a viscoelastic thin plate. The water is of constant depth. The flow under the ice is potential and linear. A boundary integral method (BIM) for the flow under the ice is combined with the finite difference method for the ice plate with free-free edge conditions to solve the coupled problem of linear hydroelasticity. Numerical results for deflections and stress distributions are shown to agree well with the available results by others. The proposed approach can be applied to problems with different edge conditions and different positions of the load with respect to the lead. The ice responses are studied with respect to the speed of the load. The speed can be subcritical, critical, and supercritical with respect to the critical speed for a floating infinite elastic plate. The speeds of the load, which provide maximum deflection, maximum stress, and maximum wave-making resistance, are determined. All these speeds are different and greater than the critical speed for an infinite elastic plate. The effect of the ice thickness, lead width, and load properties on these speeds is discussed.

Published under license by AIP Publishing. https://doi.org/10.1063/5.0037682

I. INTRODUCTION

The problem of ice-water-structure interaction received considerable attention starting from pioneering work by Kheisin (1963) and Squire et al. (1985). Comprehensive reviews of these problems were given by Squire et al. (1996) and recently by Ni et al. (2020). The latter paper reviews existing analytical, numerical, and experimental methods to solve such problems and their major applications to date. One of typical application is that of an air cushion vehicle (ACV) moving in ice covered regions. For an ACV moving on an infinite ice sheet, cracks can be induced under the ACV, which may have an obvious influence on the response and resonant behavior of the ice. In some cases, the ACV needs to move in water channels generated by an ice-breaker or various natural forces including wind, wave, and current, see Squire (2007). Therefore, it is important for ice breaking ability and safety operation of the ACV in ice covered regions to investigate the ice response to a vehicle moving either along an ice channel of constant width confined by semi-infinite ice plates on both sides of the channel or on an infinite ice sheet with a crack.

Ice response to a load moving along a floating infinite ice sheet, see Fig. 1, was well investigated. Squire et al. (1996) reviewed this

subject in full details. The steady-wave patterns and the stresses in an ice sheet caused by a pressure traveling at a constant speed were of the main concerns (Davys et al., 1985; Squire et al., 1985; and Milinazzo et al., 1995). Much attention has also been paid to time dependent results (Schulkes and Sneyd, 1988; Pogorelova and Kozin, 2010; and Dinvay et al., 2019). The developed models and obtained results make it possible to conclude whether the infinite ice sheet would be broken by the moving pressure or not by comparing the computed maximum bending stress with the so-called yield stress. Then one can either use the ice cover as an ice road in winter time or break the ice sheet by a moving hovercraft to prevent flooding on a river, for example. Kheysin (1963) could be the first researcher, who considered the problem of a load moving on a floating ice sheet. Takizawa (1985) conducted systematic field experiments with a vehicle moving on the ice sheet by measuring the deflections of the ice sheet. He determined the critical speed of the moving load, for which the deflection of the ice sheet was maximum. These experimental results are still in use to validate numerical models of ice response. Parau and Vanden-Broeck (2011) adopted BIM to study this problem including the nonlinear effects and found the critical speed of the load which provides the
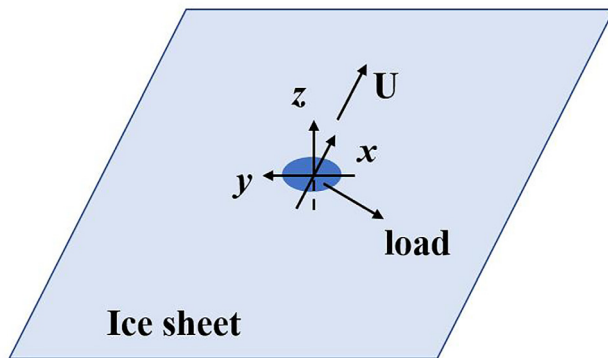
FIG. 1. Sketch of a load moving on an infinite ice sheet.

maximum deflection of ice. The linear theory of hydroelasticity without account for any dissipation predicts unbounded ice response for a so-called critical speed of the load, which is equal to the minimum of the phase speed of an uni-directional flexural-gravity waves propagating in the ice sheet (Hosking et al., 1988). At the wavenumber, for which the minimum phase speed is achieved, the phase speed and the group speed are equal. This provides a physical explanation of the unbounded response of a floating ice sheet within the linear theory of hydroelasticity for a load moving at the critical speed. Parau and Dias (2002) and Bonnefoy et al. (2009) demonstrated that the nonlinear effects made the deflection of ice near the critical speed finite. Viscoelastic models of ice also provide finite ice response at the critical speed (Takizawa, 1985 and Hosking et al., 1988). In addition, viscoelastic theory can explain the wave decay with the distance from the load (Hosking et al., 1988) and the offset of the maximum deflection position behind from the load (Takizawa, 1985). There are several viscoelastic constitutive models of ice including widely used Kelvin-Voigt model and Maxwell model (Mase, 1970). Kozin and Pogorelova (2009) studied response of viscoelastic ice to moving pressure by using the Kelvin-Voigt model, Maxwell model, and generalized Maxwell–Kelvin models. They compared their theoretical results with the experimental ones by Takizawa (1985) and concluded that the relaxation time τ should be a function of the load speed in these three models. In present study, the Kelvin-Voigt model of viscoelastic ice is used. This is one of the simplest models of viscoelastic materials.

The problems with loads moving on a semi-infinite ice sheets are more complicated than the problems for an infinite ice sheet. The edge of a floating semi-infinite ice sheet can be either clamped (frozen) to a vertical wall, see Fig. 2(a), or free-free, see Fig. 2(b), with the rest of the water surface being open. Other edge conditions are also possible. The edge conditions change significantly the ice response to a moving load. A load moving on a semi-infinite ice sheet which is clamped to a vertical wall, as shown in Fig. 2(a), was studied by Brocklehurst (2012). He studied the linear problem of a load moving at a constant distance from the wall by using Fourier transforms in both x- and y-directions, see Fig. 2(a) and Chap. 5 in Brocklehurst (2012). The ice deflection was obtained in terms of Fourier integrals, which were evaluated numerically. Different speeds of the load were considered with respect to the critical speed of the infinite ice sheet. The effect of the vertical

wall on the ice deflection for slow load speed was shown to be mostly dampening with the magnitude of the ice response being smaller due to the presence of the wall. For faster speeds, strong interaction between the wall and the generated waves was observed with significant deflections between the load and the wall. Brocklehurst (2012) also studied the same problem with a vertical wall in non-linear formulation for water of infinite depth, see Chap. 6. The plate equation was linear, but the hydrodynamic part of the problem was nonlinear. The BIM with the three-dimensional free-space Green's function, which accounts for the presence of the wall, was used. The biharmonic term in the plate equation was approximated using central finite differences. The problem was reduced to a system of nonlinear equations with respect to the values of the potential on the plate, plate deflection, and its first derivatives with respect to x and y. The system of the obtained equations was solved by Newton's method. It is not clear how this algorithm can be extended to other edge conditions, for example, free edge or simply supported edge. The numerical solution of the nonlinear problem of hydroelasticity made it possible to conclude that the speed of the load is the most important parameter of the problem. For slow speeds of the load and small distances of the load from the wall, the deflections in the wake behind the load are greater than for infinite ice sheet. This was not the case in the linear formulation.

By using the integral Fourier transform and the expansion of the speed potential with respect to the so-called vertical eigenfunctions, Sturova (2018) studied the same problem in the subcritical regime, where the speed of the load was below the critical speed for an infinite elastic ice sheet. She considered both the clamped edge and the free edge boundary conditions between the ice sheet and the vertical wall. It was found that the maximum bending moment occurred in the vicinity of the wall for the clamped edge, but it was at the center of the load region for the free edge. This proved that the boundary conditions have strong influence on the response of ice sheets.

In the problem with semi-infinite ice sheet and semi-infinite water surface, as shown in Fig. 2(b), the load can move either on the ice or on the water surface along the linear edge of the ice sheet. The ice edge is free of stresses and shear forces in this problem. By using BIM and a viscoelastic model of the ice sheet, Li et al. (2017) calculated the stress distribution and deflection of the ice sheet when the load moved either on the ice or open water. This problem, in particular, describes ice response to a boat navigating near the ice edge. However, Li et al. (2017) did not account for the free edge conditions in their analysis, which is inappropriate. The approach of the present paper properly accounts for the edge conditions. Sturova (2018) studied the problem of a load moving on a semi-infinite ice sheet in the subcritical regime. She compared the deflections of the semi-infinite ice sheet and infinite ice sheet for the same load and the same conditions. It was found that the deflection of the semi-infinite ice sheet is larger than that of the infinite ice sheet. Sturova and Tkacheva (2018) extended the analysis to the hydroelastic response of a semi-infinite ice sheet with a load moving on the water surface. They used the Fourier transform and the Wiener-Hopf technique. It was found that both the wave resistance and the side force acting on the moving load oscillated when the speed of the load was close to the critical speed of the infinite floating ice sheet.

Another related problem was formulated for a frozen channel, in other words, for an ice sheet of finite width confined by two vertical
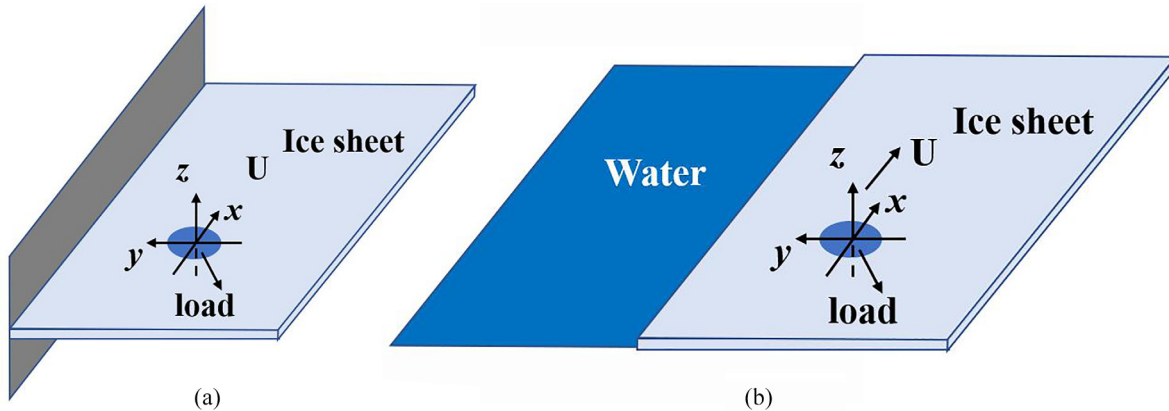
FIG. 2. Sketch of a load moving on a semi-infinite ice sheet. (a) semi-infinite ice sheet with a vertical wall, (b) semi-infinite ice sheet beside semi-infinite water surface.

walls on two sides, as shown in Fig. 3. Korobkin *et al.* (2014) studied the hydroelastic waves propagating along a frozen channel and their dispersion relations for the ice plate clamped (frozen) to the vertical walls. The linear theory of hydroelasticity and the normal mode method were used. It was found that there are infinitely many waves of the same wavelength, and correspondingly, infinitely many dispersion relations and critical speeds of these waves. The lowest critical speed for a frozen channel was shown by Shishmarev *et al.* (2016) to be higher than the critical speed for the identical infinite plate. Batyaev and Khabakhpasheva (2015) studied a similar problem but with free edge conditions between the ice and the channel wall. They also found that there are an infinite number of critical speeds, but their values of critical speeds were different from those calculated by Korobkin *et al.* (2014) for clamped edge conditions. By using these results, Shishmarev *et al.* (2016) studied the problem of a load moving along a frozen channel with clamped edge conditions at a constant speed by combining the Fourier transform along the channel with the normal mode method across the channel. The Kelvin-Voigt model of

viscoelastic ice was used. Shishmarev *et al.* (2016) were looking for the critical speeds in term of the maximum deflection, which were found to be larger than the first critical speed of the elastic ice in Korobkin *et al.* (2014). It was concluded that the viscoelastic model of ice provides maximum deflection at a speed of the load which is slightly different from the critical speed of the elastic ice. However, it was shown that the difference between the elastic and viscoelastic critical speeds decreases when the relaxation time of the viscoelastic model, see Eq. (1) below, tends to zero.

The problem of a load moving along a frozen channel within the elastic model of ice without viscoelastic effects was studied by Khabakhpasheva *et al.* (2019) for a load starting its motion from the rest and moving then with a constant speed. It was shown that the ice deflection for large times consists of several terms: time-independent deflections under the load and systems of hydroelastic waves from Korobkin *et al.* (2014) both behind and in front of the load. These hydroelastic waves move at the speed of the load and, therefore, they are standing waves in the system moving together with the load. The ice response can be caused not only by a load moving over the ice cover but also by a body moving in the channel under the ice. Such ice responses were studied by Shishmarev *et al.* (2019) using asymptotic methods and the viscoelastic model of ice for an underwater dipole. Hydroelastic waves in the channel with different edge conditions and/ or a crack along the channel were studied recently by Ren *et al.* (2020) using their own original method.

The problem with two semi-infinite ice sheets separated by a channel of open water (lead) of constant width was studied in both two-dimensional and three-dimensional formulations. Chung and Linton (2005) studied two-dimensional problem of flexural-gravity waves propagating across a lead, see Fig. 4. Shi *et al.* (2019) studied waves interact with multiple wide ice leads. Ren *et al.* (2016) studied the problem of waves propagating across a lead with a rectangular body floating in the lead by the method of matched eigenfunction expansions. It was found that the presence of ice makes the hydrodynamic coefficients of the floating body, which are functions of the frequency of incident wave, oscillate. The method is restricted to rectangular floating bodies. Li *et al.* (2017) considered floating elliptical cylinder in the lead based on wide spacing approximation. Then, Li
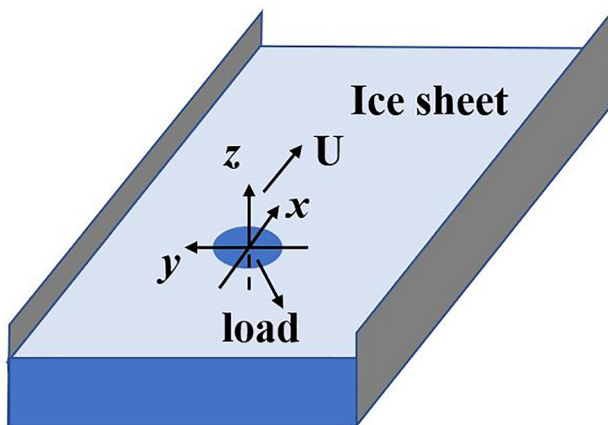

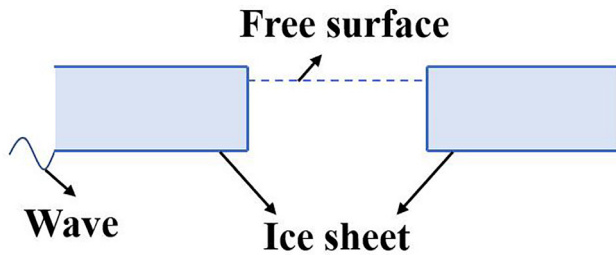**FIG. 3.** Sketch of a load moving along a frozen channel.

FIG. 4. Sketch of wave propagation across a lead.

et al. (2018a) solved the same problem by using a simple source Green function and eigenfunction matching method.

When the width of a lead approaches zero, we have a linear crack in an infinite ice sheet. Evans and Porter (2003) studied scattering of an obliquely incident flexural-gravity wave by a narrow straight-line crack separating two semi-infinite thin elastic plates floating on water of finite depth. They showed, in particular, that symmetric edge waves exist which travel along the crack and decay in a direction normal to the crack. Li *et al.* (2018b) considered a two-dimensional problem of incident flexural-gravity wave interaction with circular cylinder placed below an ice sheet with a crack. It was shown that the hydrodynamic coefficients of this cylinder oscillate as functions of the wave frequency in contrast to the coefficients determined for the ice sheet without the crack. The presence of a crack in the ice sheet has a significant effect on ice response. For three-dimensional problems of waves propagating along an ice lead or crack, Marchenko (1997) studied the dispersion relations of such waves within the shallow water approximation. Porter (2018) considered the same problem as Marchenko (1997) but for water of infinite depth. He determined the so-called edge waves, which do not penetrate the ice sheets deeply and are localized near the ice edges. He determined dispersion relations for such waves, see Fig. 3 in Porter (2018), and calculated the corresponding profiles of the waves across the lead. Tkacheva (2019a) and Sturova and Tkacheva (2019) studied the ice responses and wave forces for a load moving at a constant speed in an ice channel (lead) between two semi-infinite ice sheets. The Wiener–Hopf technique was used. Tkacheva (2019a) presented the ice sheet response for three different ice thicknesses and two load speeds. She found that the strains of the ice sheet near the edge may exceed the maximum permissible strain, so-called yield strain, for some speeds of the load, which indicates that the ice sheet can be broken near the edge by a ship moving in the lead. Tkacheva (2019b) studied also generation of waves by a load moving on infinite ice sheet with a crack within linear hydroelasticity theory. The thicknesses of the two semi-infinite ice sheets were different. The deflection of the ice sheet was analyzed for sub- and supercritical speeds of the load with respect to the critical speeds of the unbounded ice sheets with corresponding thicknesses. The deflection of the ice sheets was unbounded at the critical speeds in the solution obtained by the Wiener–Hopf technique.

In the present paper, we focus on the numerical analysis of ice response to a moving load in the presence of a lead of open water or a crack. BIM is used for this aim. The numerical results are compared with available theoretical results by others listed above. The present numerical approach is more general than the theoretical solutions,

which makes it possible to investigate practical problems with non-simplified configurations. The edge conditions are properly taken into account in the present numerical algorithm. Load speeds, which provide maximum deflection of the ice cover, maximum stress in the ice, and maximum wave-making resistance, are determined.

The formulation of the problem is given in Sec. II. The numerical algorithm is described in Sec. III. The numerical results are validated with the results by others in Sec. IV, where also new results concerning ice response are presented. The conclusions are drawn and future work is discussed in Sec. V.

II. MATHEMATICAL FORMULATION

We consider the problem of a load moving in an ice lead or on an infinite ice sheet with a crack at a constant speed U, see Fig. 5 where dimensions of both the load and the lead are introduced. A crack is treated as a lead (a channel of open water between two ice sheets) of zero width W in the present study. Below $W > 0$ for a lead and $W = 0$ for a crack. A coordinate system that moves together with the external load along the lead is used, see Fig. 5. The origin O of the system is located at the center of the external load, which is symmetric in both the x-direction along the lead and in the y-direction across the lead. The z-axis points upwards, opposite to the gravitational acceleration $\vec{g}$. The water is of constant depth H, see Fig. 5. The fluid is assumed to be inviscid and incompressible, and the flow is irrotational. The ice sheet is assumed of infinite extent and homogeneous with thickness h and rigidity $D = Eh^3[12(1 - \nu^2)]$, where E is Young's modulus of the ice and ν is Poisson's ratio of the ice. The deflection of the ice sheet is described by the thin viscoelastic Kelvin–Voigt plate model (Mase, 1970). The edges of the ice sheet along the lead and/or crack are free of stresses and shear forces. The draft of the ice sheet is neglected in this study with the ice thickness h being much smaller than the water depth H. The external load is modeled by a localized smooth pressure $P(x, y)$ with characteristic length L along the lead and B across the lead, see Fig. 5. The pressure $P(x, y)$ is even in x and y. The pressure is applied over the water surface for ice lead and over the upper surface of the ice sheet for infinite ice sheet with the crack along $y = 0$. We shall determine the time-independent flow and ice deflection in the moving coordinate system.

The ice deflection and the free-surface elevation are described by the equation $z = \eta(x, y)$, where $\eta(x, y)$ is a solution of the viscoelastic plate equation written in the moving coordinates (Mase, 1970)

$$D\left(1 - \tau U \frac{\partial}{\partial x}\right)\nabla^4\eta + \rho_i h U^2 \frac{\partial^2 \eta}{\partial x^2}$$
$$= p(x, y, 0) - P(x, y) \quad (|x| < \infty, |y| < \infty), \quad (1)$$

where $h = 0$ and $D = 0$ in open water, $-W/2 < y < W/2$, $\tau = \mu/E$ is the relaxation time, μ is the viscosity of ice, $\nabla^4 = \partial^4/\partial x^4 + 2\partial^4/(\partial x^2\partial y^2) + \partial^4/\partial y^4$ is the biharmonic operator, ρ_i is the density of ice, which is taken as $\rho_i = 900 \, \text{kg/m}^3$ in this study, and $p(x, y, 0)$ is the hydrodynamic pressure. Note that Eq. (1) is the plate equation only in $|y| > W/2$. In $|y| < W/2$, the left-hand side of (1) is zero and the equation represents the dynamic boundary condition for open water.

The external pressure $P(x, y)$ is described in this study by (Doctors and Sharma, 1972)

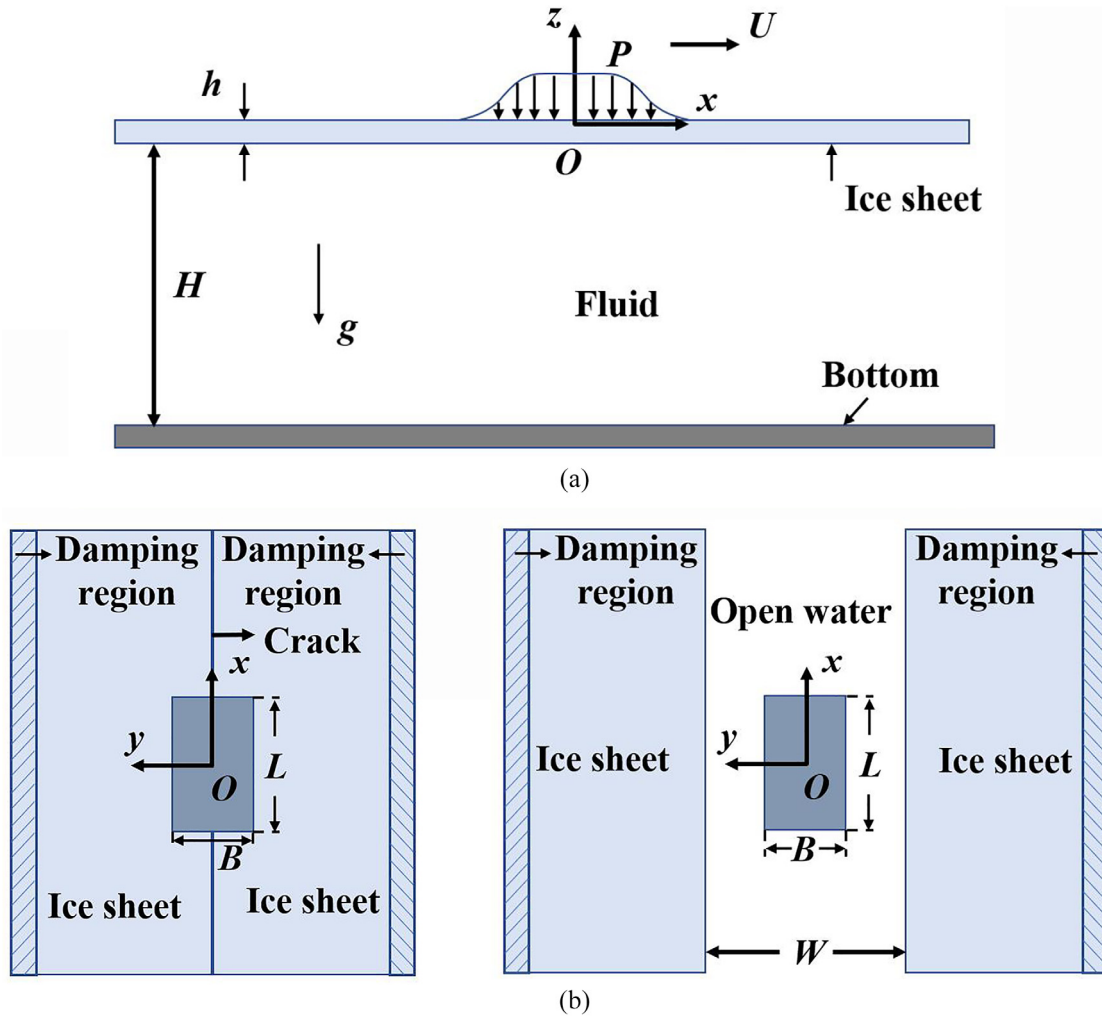$$P(x, y) = P_0 S(\alpha, 2x/L) S(\beta, 2y/B), \quad (2)$$

FIG. 5. Sketch of a load moving in an ice lead or on an infinite ice sheet with a crack at a constant speed: (a) side view, (b) top view (lead), and (c) top view (crack).

$$S(\alpha, 2x/L) = \frac{1}{2}\left\{\tanh\left[\alpha\left(\frac{2x}{L}+1\right)\right] - \tanh\left[\alpha\left(\frac{2x}{L}-1\right)\right]\right\},$$

$$S(\beta, 2y/B) = \frac{1}{2}\left\{\tanh\left[\beta\left(\frac{2y}{B}+1\right)\right] - \tanh\left[\beta\left(\frac{2y}{B}-1\right)\right]\right\},$$

where P is the equivalent pressure over the area LB, which provides the same total load as (2), and α and β are dimensionless parameters which control the pressure decay with the distance from the pressure center. The limiting case with $\alpha \to \infty$ and $\beta \to \infty$ corresponds to a uniform pressure acting over the rectangular area: $|x| \le L/2$, $|y| \le B/2$. It is known that such a uniform pressure moving over a water surface provides a wave-resistance with unrealistic oscillations at low Froude numbers; see Doctors and Sharma (1972) for details. In practice, it takes a finite distance for the pressure at the edge of the ACV to drop to zero gradually rather than suddenly (Doctors and Sharma, 1972). The function $S(\alpha, 2x/L)$ is even and positive, and monotonically decays from $\tanh(\alpha)$ at $x = 0$ to zero as $x \to \infty$.

The conditions that the ice edges are free of stresses and shear forces read

$$\left(\frac{\partial^2}{\partial y^2} + \nu\frac{\partial^2}{\partial x^2}\right)\eta = 0, \quad \frac{\partial}{\partial y}\left(\frac{\partial^2}{\partial y^2} + (2-\nu)\frac{\partial^2}{\partial x^2}\right)\eta = 0$$

$$\left(|x| < \infty, y = -\frac{W}{2} - 0 \quad \text{and} \quad y = \frac{W}{2} + 0\right). \quad (3)$$

Note that the free-surface elevation, $z = \eta(x,y)$, where $|y| < W/2$, and the ice deflection, which is described by the same equation but where $|y| > W/2$, are not continuous, in general, at the ice edges,

$$\eta\left(x, \pm\frac{W}{2} - 0\right) \neq \eta\left(x, \pm\frac{W}{2} + 0\right),$$

together with their derivatives. On the other hand, for the crack, due to the symmetry of the problem, $\eta(x,y)$ is continuous but not differentiable at $y = 0$.

The hydrodynamic pressure $p(x, y, 0)$ on the upper boundary of the fluid in the moving coordinate system is given by the linearized Bernoulli equation

$$p(x, y, 0) = \rho_w U \frac{\partial \varphi}{\partial x} - \rho_w g \eta \quad (|x| < \infty, |y| < \infty, z = 0), \quad (4)$$

where ρ_w is the density of water taken as $\rho_w = 1000 \, \text{kg/m}^3$ in this paper, $\varphi(x, y, z)$ is the velocity potential, which satisfies Laplace's equation in the flow region,

$$\frac{\partial^2 \varphi}{\partial x^2} + \frac{\partial^2 \varphi}{\partial y^2} + \frac{\partial^2 \varphi}{\partial z^2} = 0 \quad (|x| < \infty, |y| < \infty, -H < z < 0), \quad (5)$$

the linearized kinematic boundary condition on the upper surface,

$$\frac{\partial \varphi}{\partial z} = -U \frac{\partial \eta}{\partial x} \quad (|x| < \infty, |y| < \infty, z = 0), \quad (6)$$

and the bottom boundary condition,

$$\frac{\partial \varphi}{\partial z} = 0 \quad (z = -H). \quad (7)$$

The deflections and the flow generated by the moving load within the model of viscoelastic ice plate decay with the distance from the load,

$$\eta \to 0, \quad \varphi \to 0 \quad (|x| \to \infty, |y| \to \infty). \quad (8)$$

The wave resistance R_w acting on the moving load is given by (Doctors and Sharma, 1972)

$$R_w = \int_{-\infty}^{+\infty} \int_{-\infty}^{+\infty} P(x, y) \frac{\partial \eta}{\partial x}(x, y) \, dx dy. \quad (9)$$

The non-dimensional resistance coefficient C_w is defined by

$$C_w = \frac{R_w \rho_w g}{P_0^2 L}. \quad (10)$$

The stress distribution in the ice sheet is of particular concern. It is of practical interest to know whether a load moving in the lead can generate stresses in the ice sheet which are large enough to break the ice. In the linear theory of hydroelasticity, the bending stresses vary linearly through the ice thickness being zero at the middle of the plate thickness. At any location, the maximum stress is achieved at the upper or lower surface of the ice plate. Considering that the absolute values of the stresses at the upper and lower surfaces are the same, we are just concerned with the stress at the upper surface of the ice

$$\begin{pmatrix} \sigma_{xx} \\ \sigma_{yy} \\ \sigma_{xy} \end{pmatrix} = \frac{Eh}{2(1-\nu^2)} \left(1 - \tau U \frac{\partial}{\partial x}\right) \begin{pmatrix} \dfrac{\partial^2 \eta}{\partial x^2} + \nu \dfrac{\partial^2 \eta}{\partial y^2} \\ \nu \dfrac{\partial^2 \eta}{\partial x^2} + \dfrac{\partial^2 \eta}{\partial y^2} \\ (1-\nu) \dfrac{\partial^2 \eta}{\partial x \partial y} \end{pmatrix}. \quad (11)$$

The flow domain and the ice sheets are of infinite extent which makes the problem complicated for analysis. However, the viscoelastic model of ice introduces damping responsible for fast decay of the solution with distance from the load. The present problem is solved numerically for a finite region around the load. The numerical region is wide enough, which makes the numerical solution practically independent of the dimensions of the region.

A special attention is paid to the edge conditions (3) in the present numerical solution.

The problem (1)–(11) cannot be used for $\tau = 0$. The numerical domain should be large for small τ in order to arrive at the converging solution. For $\tau = 0$, other approaches should be used, see Khabakhpasheva *et al.* (2019), for example.

III. NUMERICAL METHOD

The boundary problem (1)–(8) is solved by the Boundary Integral Method (BIM) using a Rankine source for a half-space $z > -H$. The Rankine sources are distributed around the load and slightly above the upper boundary of the flow region, at $z = z_0 > 0$. The plane $z = z_0$ is covered with small rectangular panels. The strength of the Rankine source is approximated as constant at each panel. In this way, the velocity potential, its first derivatives, and the hydrodynamic pressure at $z = 0$ are approximated by finite series of smooth functions with unknown coefficients. The kinematic condition (6), the edge conditions (3), and the plate equation (1), where the external pressure, $P(x, y)$, is given, provide an algebraic system for unknown coefficients through the collocation method.

In the BIM, the velocity potential $\varphi(x, y, z)$ is sought in the following form:

$$\varphi(x, y, z) = \int_{-\infty}^{+\infty} \int_{-\infty}^{+\infty} \sigma(x_0, y_0) \left(\frac{1}{r} + \frac{1}{r'}\right) dx_0 dy_0, \quad (12)$$

where $r = \sqrt{(x - x_0)^2 + (y - y_0)^2 + (z - z_0)^2}$, $r' = \sqrt{(x - x_0)^2 + (y - y_0)^2 + (z + z_0 + 2H)^2}$, and the function $\sigma(x_0, y_0)$ is to be determined. The potential (12) satisfies Laplace's equation (5), the bottom boundary condition (7), and decays at infinity. Here z_0 is a small positive number, such that $r \neq 0$ and $r' \neq 0$ at any point of the flow region including its boundary $z = 0$.

Distributions of panels and control points are shown in Fig. 6. The surface of integration in (12), $z = z_0 = c_1 \Delta x$, is limited to $-L_{bx} < x_0 < L_{fx}$ and $-L_y < y_0 < L_y$, where both L_{bx}, L_{fx}, L_y are large enough compared with the width of the lead W and the load dimensions, L and B, and discretized into small rectangular panels with m panels in the x-direction and n panels in the y-direction. The dimensions of the panels are $\Delta x = (L_{bx} + L_{fx})/m$ and $\Delta y = 2L_y/n$ in the x- and y-directions, respectively. The coefficient c_1 is taken usually between 1 and 3 based on numerical experience (Raven, 1996). Control points are placed on $z = 0$ under the center of each panel and moved a short distance $c_2 \Delta x$ forward, in the direction of the load motion. In this way, the control points are uniformly spaced, with intervals Δx and Δy in the x- and y-directions, respectively, between control points. The shift $c_2 \Delta x$, where $c_2 < 1$, improves stability of the numerical solution (Raven, 1996). In the present simulations, we take $c_2 = 0.15$. The relative positions of the panels and the control points are shown in Fig. 7.

We number the panels and the corresponding control points by $j = (k-1)m + l$, where $l = 1, 2, \ldots, m$ is the number of the panel in the x-direction and $k = 1, 2, \ldots, n$ is the number of the panel in the y-direction. Note that j and pairs (l, k) correspond one-to-one for given n and m. The function $\sigma(x_0, y_0)$ in (12) is approximated as constant, $\sigma = \sigma_j$, on the jth panel S_j, where $-L_{bx} + (l-1)\Delta x < x_0 < -L_{bx}$
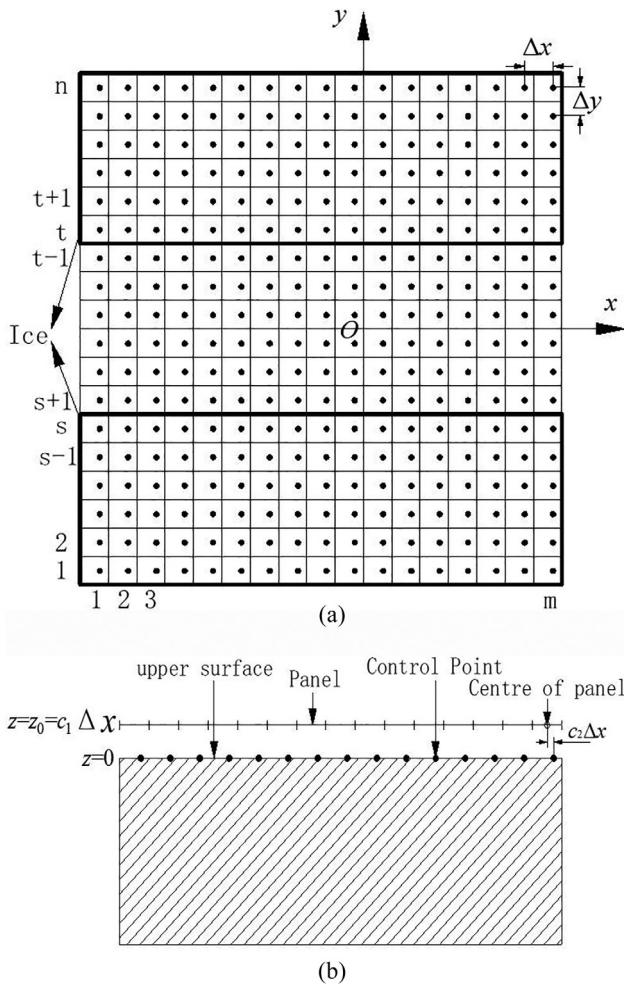
FIG. 6. Distributions of panels and control points: (a) top view and (b) side view.

$+l\Delta x$ and $-L_y + (k-1)\Delta y < y_0 < -L_y + k\Delta y$. Then, the velocity potential at the ith control point, $\varphi_i = \varphi(x_i, y_i, 0)$, is given by

$$\varphi_i = \sum_{j=1}^{m\times n} \sigma_j \Phi_{i,j}, \quad \Phi_{i,j} = \iint_{S_j} \left(\frac{1}{r_i} + \frac{1}{r'_i} \right) dx_0 dy_0, \quad (13)$$
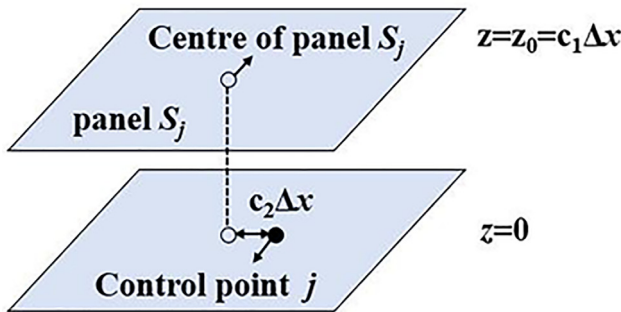

FIG. 7. Relative positions of the jth panel and jth control point on the upper surface of the flow region.

where $\qquad r_i = \sqrt{(x_i - x_0)^2 + (y_i - y_0)^2 + z_0^2}$, $\qquad r'_i$
$= \sqrt{(x_i - x_0)^2 + (y_i - y_0)^2 + (z_0 + 2H)^2}$, $\quad i = (p-1)m + q$,
$p = 1, 2, \ldots, n$, $\quad q = 1, 2, \ldots, m$ and $\quad x_i = -L_{bx} + (q-1)\Delta x$
$+ 0.5\Delta x + c_2\Delta x$, $\; y_i = -L_y + (p-1)\Delta y + 0.5\Delta y$. The derivative $\partial\varphi(x_i, y_i, 0)/\partial z = \varphi_{z,i}$ at the ith control point is given by

$$\varphi_{z,i} = \sum_{j=1}^{m\times n} \sigma_j \Psi_{i,j}, \quad \Psi_{i,j} = \iint_{S_j} \left(\frac{z_0}{r_i^3} - \frac{z_0 + 2H}{r'_i{}^3} \right) dx_0 dy_0. \quad (14)$$

The integral $\Phi_{i,j}$ and $\Psi_{i,j}$ are calculated by the Hess–Smith method (Hess and Smith, 1964).

The elevation of the upper surface of the flow region, $\eta(x, y)$, is obtained from (6) and (8)

$$\eta(x, y) = \frac{1}{U} \int_x^\infty \frac{\partial\varphi}{\partial z}(\tilde{x}, y, 0) \, d\tilde{x},$$

where the integral is evaluated by the trapezoidal rule. At the ith control point, we have

$$\eta_i = \frac{1}{U} \int_{x_i}^\infty \frac{\partial\varphi}{\partial z}(\tilde{x}, y_i, 0) \, d\tilde{x}$$

$$\approx \frac{\Delta x}{U} \left[\frac{1}{2}\varphi_{z,i} + \sum_{l=q+1}^{m-1} \varphi_{z,(p-1)m+l} + \frac{1}{2}\varphi_{z,pm} \right], \quad (15)$$

where $\eta_i = 0$ for $q = m$. Equations (14) and (15) provide

$$\eta_i = \frac{\Delta x}{U} \sum_{j=1}^{m\times n} \sigma_j \left\{ \frac{1}{2}\Psi_{i,j} + \sum_{l=q+1}^{m-1} \Psi_{(p-1)m+l,j} + \Psi_{pm,j} \right\} = \sum_{j=1}^{m\times n} \sigma_j E_{i,j}, \quad (16)$$

where $1 \leq i \leq nm$ and $E_{i,j}$ depend on z_0, H, Δx, and Δy for a given panel j and a given control point i.

The x-derivative $\partial\varphi(x, y, 0)/\partial x$ in (4) is calculated by the upstream finite difference

$$\varphi_{x,i} = \begin{cases} \dfrac{-3\varphi_i + 4\varphi_{i+1} - \varphi_{i+2}}{2\Delta x} & q < m-1, \\[2mm] \dfrac{\varphi_{i+1} - \varphi_i}{\Delta x} & q = m-1, \\[2mm] \dfrac{\varphi_i - \varphi_{i-1}}{\Delta x} & q = m, \end{cases} \quad (17)$$

which reasonably well fits the radiation condition far from the moving load, see Letcher (1993) and Liu et al. (2013) for more details and discussions. The second x-derivative $\partial^2\eta/\partial x^2$ in (1) is calculated using (6), $\eta_{xx} = -\varphi_{zx}(x, y, 0)/U$, and (17)

$$\eta_{xx,i} = -\frac{1}{U} \begin{cases} \dfrac{-3\varphi_{z,i} + 4\varphi_{z,i+1} - \varphi_{z,i+2}}{2\Delta x} & q < m-1, \\[2mm] \dfrac{\varphi_{z,i+1} - \varphi_{z,i}}{\Delta x} & q = m-1, \\[2mm] \dfrac{\varphi_{z,i} - \varphi_{z,i-1}}{\Delta x} & q = m. \end{cases} \quad (18)$$

This second derivative is needed only for the control points on the ice surface, where $1 \leq p \leq s$ and $t \leq p \leq n$, see Fig. 6(a). Note that $s + 1 = t$ for $W = 0$, which is for the problem with a crack.

In order to calculate the biharmonic term $\nabla^4\eta$, which is needed only for the control points on the ice plate, we divide it into three terms, $\partial^4\eta/\partial x^4$, $\partial^4\eta/\partial y^4$, and $\partial^4\eta/(\partial x^2\partial y^2)$. The first term, $\partial^4\eta/\partial x^4$, at the control points on the ice surface with $q = 3$, $4, \ldots, m-2$ is approximated using the central finite differences with 5 points. For the control points with $q = 1, 2$ and $m-1$, m, which are near the boundary of the calculation domain, $\partial^4\eta/\partial x^4$ is approximated using the same finite differences as the control points with $q = 3$ and $m-2$, respectively. The second term, $\partial^4\eta/\partial y^4$, at the control points on the ice surface with $p = 3, 4, \ldots, s-2$ and $p = t+2$, $t+3 \cdots, n-2$ is approximated using the central finite differences with 5 points. For the control points with $p = 1, 2$ and $n-1$, n, which are near the boundary of the calculation domain, $\partial^4\eta/\partial y^4$ is approximated using the same finite differences as the control points with $p = 3$ and $n-2$, respectively. To calculate $\partial^4\eta/\partial y^4$ near the ice edges, we introduce two layers of fictitious control points outside the ice edges, as it is shown in Fig. 8 (Ertekin and Xia, 2014) and new unknowns, which are considered as deflections of the fictitious points, η_r, with numbers $r = (n-1+u)m+q$, where $q = 1, 2, \ldots, m$ and $u = 1, 2, 3, 4$. In this way, the term $\partial^4\eta/\partial y^4$ at the control points with $p = s-1, s, t$ and $t+1$, is also approximated using the central finite differences with 5 points, see Figs. 9(a) and 9(b), using $4m$ extra unknowns. The term $\partial^4\eta/(\partial x^2\partial y^2)$ at the control points with $p = 2$, $3, \ldots, s-1$ and $p = t+1, t+2, \ldots, n-1$, where $q = 2, 3, \ldots$, $m-1$, is approximated using the central finite differences with 9 points. For the control points with $p=1$ and n, where $q = 2$, $3, \ldots, m-1$, $\partial^4\eta/(\partial x^2\partial y^2)$ is approximated using the same finite differences as the control points with $p = 2$ and $n-1$, where $q = 2, 3, \ldots, m-1$, respectively. For the control points with $p = s$ and $p = t$, where $q = 2, 3, \ldots, m-1$, $\partial^4\eta/(\partial x^2\partial y^2)$ is also approximated using the central finite differences with 9 points, see Fig. 9(c). For the control

points on the ice surface with $q = 1$ and m, $\partial^4\eta/(\partial x^2\partial y^2)$ is approximated using the same finite differences as the control points with $q = 2$ and $m-1$, respectively. Therefore, in the present approximation, we have $4m$ more unknowns η_r, in addition to $n \times m$ unknowns σ_j, and we calculate the term $\nabla^4\eta$ at any control points on the ice surface by the 13-points scheme through $n \times m$ deflections η_i of the ice, which are related to the σ_j by (16), and $4m$ fictitious deflections η_r, which are unknowns on their own. Additional $4m$ equations for the extra $4m$ unknowns η_r will be obtained below using the conditions at the ice edges. The relative positions of the control points, fictitious points, and interpolating points are shown in Figs. 8 and 10.

The x-derivative of the biharmonic term $\partial(\nabla^4\eta)/\partial x = \nabla^4$ $(\partial\eta/\partial x)$, which comes from the damping term in the plate equation (1), is needed at each control point on the ice plate. This term is approximated in the same way as the term $\nabla^4\eta$, see above, where η_x is approximated using (6), $\partial\eta/\partial x = -(\partial\varphi/\partial z)/U$, and (14) at the control points of the ice plate, and by the finite differences at the fictitious points

$$
\left(\frac{\partial\eta}{\partial x}\right)_r = \begin{cases} \dfrac{\eta_{r+1}-\eta_{r-1}}{2\Delta x} & 1 < q < m, \\[2ex] \dfrac{\eta_{r+1}-\eta_r}{\Delta x} & q = 1, \\[2ex] \dfrac{\eta_r-\eta_{r-1}}{\Delta x} & q = m. \end{cases}
$$

We require that Eq. (1) is satisfied at each control point

$$
D\left(1-\tau U\frac{\partial}{\partial x}\right)\nabla^4\eta_i - \rho_i hU\left(\frac{\partial^2\eta}{\partial x^2}\right)_i - \rho_w U\left(\frac{\partial\varphi}{\partial x}\right)_i + \frac{\rho_w g}{U}\eta_i = -P_i,
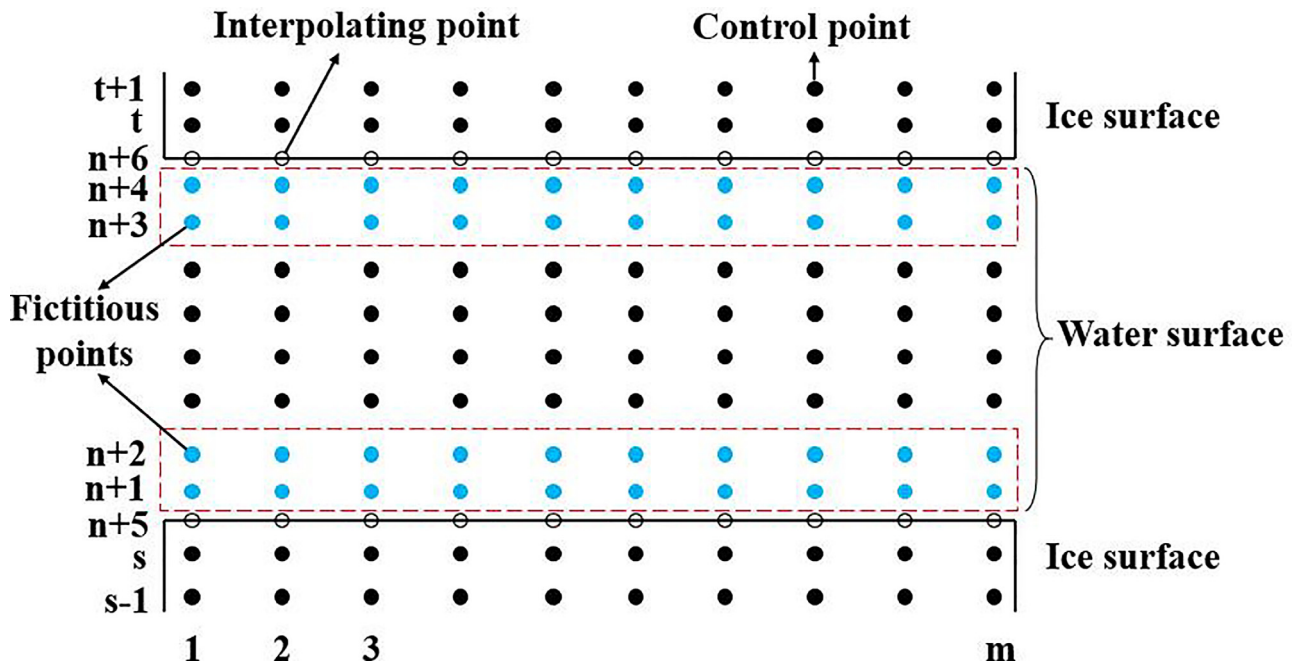$$

$$\tag{19}$$

FIG. 8. Relative positions of the control points, fictitious points, and interpolating points (top view).
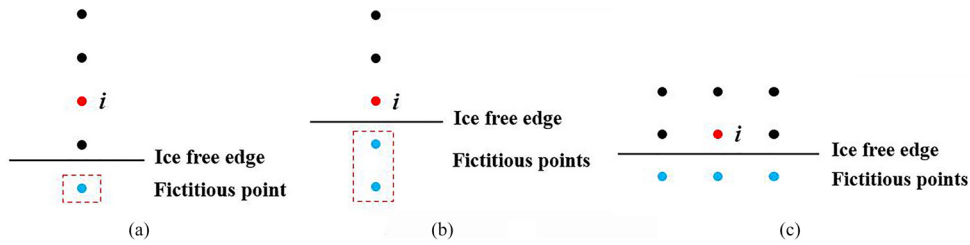
FIG. 9. The control and fictitious points used in calculations of the fourth derivative with respect to y [(a) and (b)] and in calculations of the derivative $(\partial^4\eta/(\partial x^2\partial y^2))_i$ near the ice edge (c).

where $i = (p-1)m + q$, $p = 1, 2, \ldots, n$, $q = 1, 2, \ldots, m$, and $P_i = P(x_i, y_i)$. Each term in (19) is approximated by finite differences, as explained above, and expressed through σ_j and η_r. For $s < p < t$, see Fig. 8, the control points are located on the water surface, where $D = 0$ and $h = 0$. Equation (19) provides $m \times n$ linear equations with $m \times n + 4m$ unknowns. Additional $4m$ equations follow from the edge conditions (3). These conditions are imposed at the ice edges, which are on the boundaries between panels, see Fig. 6(a). The edge conditions are satisfied at interpolation points, see Fig. 8, which are placed along the ice edges. We introduce the deflections of the interpolation points, η_d, with numbers $d = (n-1+e)m + q$, where $q = 1, 2, \ldots, m$ and $e = 5, 6$. The deflection of the interpolating points is calculated by using three-point Lagrange extrapolation function

$$\eta_d = \begin{cases} \dfrac{15}{8}\eta_i - \dfrac{5}{4}\eta_{i-m} + \dfrac{3}{8}\eta_{i-2m} & (e=5, p=s) \\[2mm] \dfrac{15}{8}\eta_i - \dfrac{5}{4}\eta_{i+m} + \dfrac{3}{8}\eta_{i+2m} & (e=6, p=t) \end{cases}.$$

where $i = (p-1)m + q$, $q = 1, 2, \ldots, m$. Applying edge conditions (3) to dth interpolating points at the ice edges, one can obtain

$$\left(\frac{\partial^2\eta}{\partial y^2}\right) + \nu\left(\frac{\partial^2\eta}{\partial x^2}\right)_d = 0 \quad \left(\frac{\partial^3\eta}{\partial y^3}\right)_d + (2-\nu)\left(\frac{\partial^3\eta}{\partial x^2\partial y}\right)_d = 0. \quad (20)$$

where for $e = 5$,

FIG. 10. Relative positions of the control points, fictitious points and interpolating points (side view).

$$\begin{cases} \left(\dfrac{\partial^2\eta}{\partial y^2}\right)_d = \dfrac{4}{(\Delta y)^2}(\eta_i - 2\eta_d + \eta_r) \\[2mm] \left(\dfrac{\partial^2\eta}{\partial x^2}\right)_d = \dfrac{\eta_{d+1} - 2\eta_d + \eta_{d-1}}{(\Delta x)^2}, \\[2mm] \left(\dfrac{\partial^3\eta}{\partial y^3}\right)_d = \dfrac{2}{(\Delta y)^3}(3\eta_i - \eta_{i-m} - 3\eta_r + \eta_{r+m}) \\[2mm] \left(\dfrac{\partial^3\eta}{\partial x^2\partial y}\right)_d = \dfrac{\eta_{r+1} - \eta_{i+1} - 2(\eta_r - \eta_i) + \eta_{r-1} - \eta_{i-1}}{\Delta y(\Delta x)^2} \end{cases} \quad (p=s, u=1),$$

for $e = 6$,

$$\begin{cases} \left(\dfrac{\partial^2\eta}{\partial y^2}\right)_d = \dfrac{4}{(\Delta y)^2}(\eta_i - 2\eta_d + \eta_r) \\[2mm] \left(\dfrac{\partial^2\eta}{\partial x^2}\right)_d = \dfrac{\eta_{d+1} - 2\eta_d + \eta_{d-1}}{(\Delta x)^2}, \\[2mm] \left(\dfrac{\partial^3\eta}{\partial y^3}\right)_d = \dfrac{2}{(\Delta y)^3}(-3\eta_i + \eta_{i+m} + 3\eta_r - \eta_{r-m}) \\[2mm] \left(\dfrac{\partial^3\eta}{\partial x^2\partial y}\right)_d = \dfrac{\eta_{i+1} - \eta_{r+1} - 2(\eta_i - \eta_r) + \eta_{i-1} - \eta_{r-1}}{\Delta y(\Delta x)^2} \end{cases} \quad (p=t, u=4).$$

Equation (20) provides the additional $4m$ equations. In this way, Eqs. (19) and (20) give $m \times n + 4m$ equations for $m \times n + 4m$ unknowns in total. The described numerical algorithm is applied below to the problems of pressure moving either along the ice lead or on infinite ice sheet with a crack.

For a lead of non-zero width, water waves propagate along the lead in both directions from the moving load with small dissipation even for a viscoelastic model of ice. Such waves are well described numerically by using the upstream finite difference scheme (17). To avoid large computational domains in the y-directions, and to enforce the far-field condition (8) as $|y| \to \infty$, damping regions are introduced near the ends of the computational domain and far from the ice edge, see Figs. 5(b) and 5(c). In these regions, a dissipative term $\upsilon\varphi_i$ is added to the left-hand side of Eq. (19), where υ is a positive coefficient of artificial viscosity, see Parau et al. (2007) for details of this approach. The value of the coefficient υ depends on the load speed. The
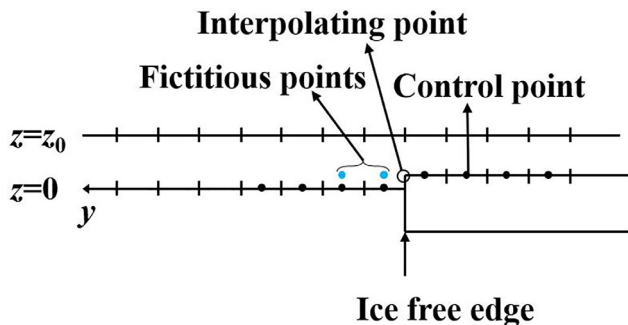
TABLE I. The parameters used for simulation.

	Case 1	Case 2	Case 3	Case 4
L (m)	20	20	40	40
B (m)	10	10	20	20
α	5	5	∞	5
β	2.5	2.5	∞	2.5
P_0 (Pa)	1000	1000	1000	1000
H (m)	Infinite	6	350	100
h (m)	…	0.2	2.5	0.4
ν	…	1/3	1/3	1/3
E (N/m^2)	…	5×10^9	5×10^9	5×10^9
τ(s)	…	1	0	0.7

dissipative term in the damping regions is responsible for smooth decay of the ice deflection there without reflection waves from these regions caused by the sudden change in viscous damping.

IV. VALIDATION OF THE ALGORITHM

In order to validate the present numerical algorithm, we compare our numerical results with available theoretical results of others. Three problems are considered for validation.

The first problem (case 1) deals with a pressure moving on open water without ice. This problem was studied by Doctors and Sharma (1972) for the conditions listed in the first column of Table I. Our numerical algorithm was applied to this problem with the following parameters of calculations: $L_{bx} = 5L$, $L_{fx} = 3L$, $L_y = 2.5L$, $\Delta x = 0.2$ m, and $\Delta y = 2$ m. The mesh size in the y direction is much larger than in the x direction, because, in this problem, there are no y-derivatives in the boundary conditions. No artificial dissipation on the free surface is used in our calculations. The far-field condition of outgoing waves is satisfied by using the upstream finite difference scheme (17). Our numerical results are compared well with the theoretical results by Doctors and Sharma (1972) in Fig. 11 in terms of the wave-making resistance coefficient in deep water.
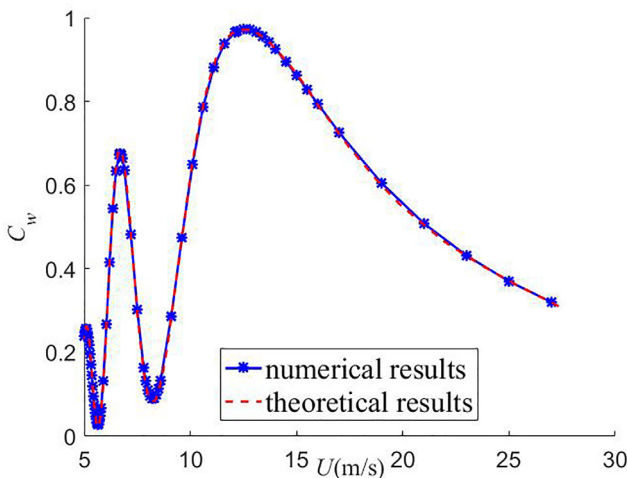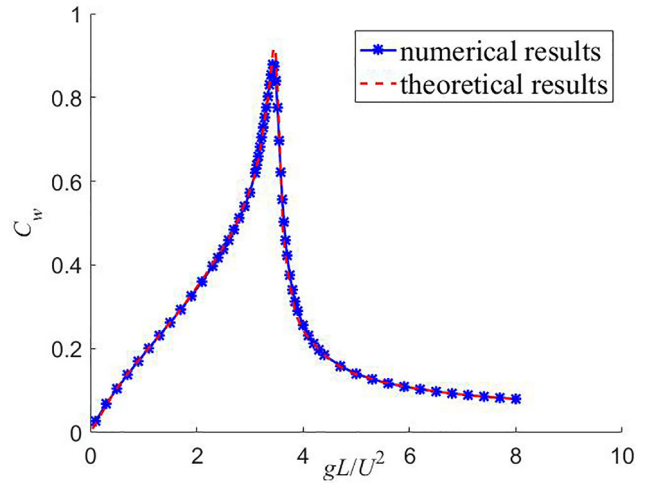
FIG. 12. Wave-making resistance coefficient for infinite ice sheet from Kozin and Pogorelova (2003).

The second problem (case 2) is concerned with a pressure moving on the ice surface of infinite extend. This problem was studied by Kozin and Pogorelova (2003) for the conditions listed in the second column of Table I. Our numerical algorithm was applied to this problem with the following parameters of calculations: $L_{bx} = 8L$, $L_{fx} = 5L$, $L_y = 6.5L$, $\Delta x = \frac{5}{3}$ m, and $\Delta y = 2$ m. Our numerical results agree well with the theoretical solution of Kozin and Pogorelova (2003) in terms of the wave-making resistance coefficient for infinite ice sheet, see Fig. 12.

The third problem (case 3) deals with a uniform rectangular load moving on the semi-infinite elastic ice sheet beside the semi-infinite water surface. This problem was studied by Sturova (2018) for the conditions listed in the third column of Table I. Note that $\tau = 0$ in this
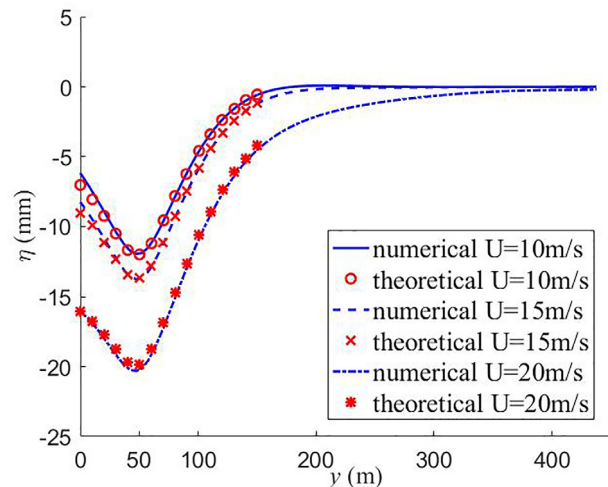
FIG. 11. Wave-making resistance coefficient for deep open water from Doctors and Sharma (1972).

FIG. 13. Profiles of semi-infinite ice calculated theoretically by Sturova (2018) for three different speeds of the load moving along the ice edge. Numerical results are obtained by the present algorithm.

problem. In order to satisfy the far-field condition (8) numerically in our solution, a dissipative term $\upsilon\varphi_i$ is introduced in damping regions far from the ice edge, see Figs. 2(b) and 5(b). The distance between the center of the load and the ice edge is 50m. Our numerical algorithm was applied to this problem with the following parameters of calculations: $L_{bx} = L_{fx} = 11L$, $L_y = 11L$, $\Delta x = 5m$, and $\Delta y = 5m$. The deflections of the ice sheet are compared with the theoretical solution of Sturova (2018) for three speeds of the load, 10m/s, 15m/s, and 20m/s in Fig. 13. One can see that the numerical results are in good agreement with the theoretical results. Different from two other problems, this case involves the free edge of ice sheet. Therefore, the demonstrated good agreement further validates the numerical scheme proposed in this paper to solve properly the problems for floating ice sheets with free edges.

After the validation of the algorithm, two following problems are investigated: (1) pressure moving along an ice lead, see Sec. V, and (2) pressure moving on the ice sheet with a crack, see Sec. VI. The conditions of these two problems are presented in the fourth column (case 4) of Table I. The numerical algorithm for these two problems is applied with the following parameters of calculation: $L_{bx} = 8L$, $L_{fx} = 5L$, $L_y = 6.5L$, $\Delta x = \frac{8}{3}$ m, and $\Delta y = \frac{10}{3}$ m.

V. PRESSURE MOVING IN ICE LEAD

This problem is studied for the external moving pressure given by Eq. (2), where dimensionless parameters α and β control how quickly the load decays with the distance from the center of the load. We assume that the pressure moving along a lead models an air cushion vehicle of rectangular shape. Then the equivalent moving load is almost constant under the ship and quickly decays with distance from
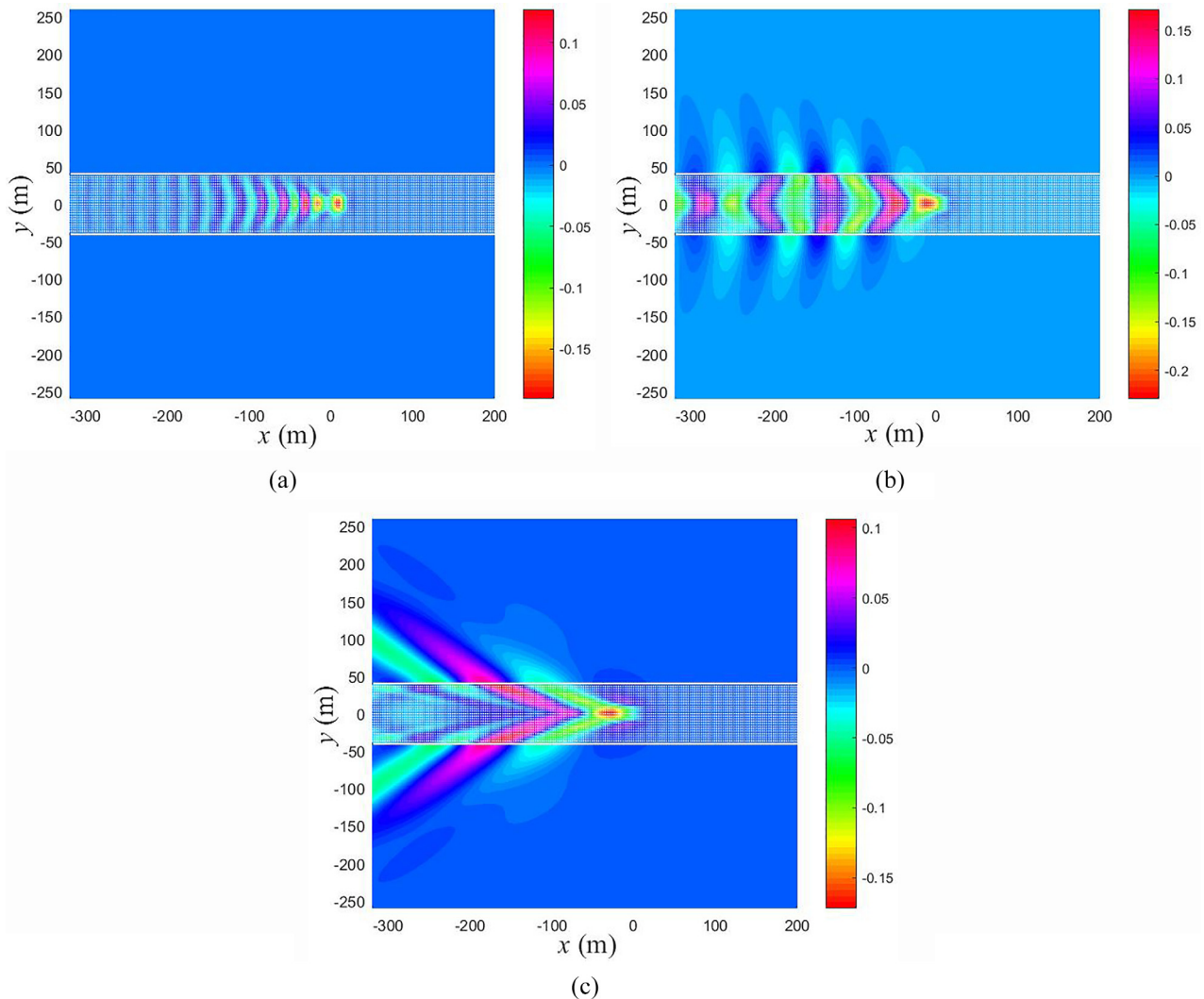

FIG. 14. Three-dimensional free surface elevation and ice deflection for three speeds U of the load: (a) subcritical case, $U = 6\,\text{m/s}$; (b) critical case, $U_{cr}^{\infty} = 11.1\,\text{m/s}$; and (c) supercritical case, $U = 20\,\text{m/s}$.

the ship. If the ship does not touch the ice on the sides of the lead, then the parameters α and β cannot be too small. They also cannot be large in order to avoid the difficulties with sharp edges of the external pressure on a free surface, see Doctors and Sharma (1972). As a result, we use $2 \leq \alpha, \beta \leq 10$ in the present method. Other parameters are given by case 4 in Table I.

A. Effect of the load speed

The minimum phase speed of flexural-gravity waves of small amplitude in an infinite elastic ice sheet for the parameters of this paper is equal approximately to 11.1 m/s, which as the critical speed of a load U_{cr}^{∞}, at which the deflection of the infinite elastic ice sheet becomes unbounded (Hosking *et al.*, 1988) if the viscous properties of ice are not accounted, $\tau \to 0$. Subcritical speed region, critical speed,

and supercritical speed region are defined with respect to U_{cr}^{∞}. Note that the critical speed or critical speeds of the ice sheets with a lead between them could be different from U_{cr}^{∞}. However, in this study, the value U_{cr}^{∞}, which is independent of both the width of the lead and the width of the channel, is used as the reference speed. We calculate deflections of the ice sheets and elevation of the water surface in the lead for subcritical, critical and supercritical speeds of the load and characteristics of the ice listed above.

The shapes of the upper surface of the flow region for three different speeds of the load are shown in Fig. 14. It can be seen that for the subcritical case the water surface oscillates relatively regularly, the amplitude of the waves gradually decreases with the distance from the load, and the ice sheet remains almost flat. Differently from the subcritical case, ice sheets oscillate visibly for both critical and supercritical cases. The water surface elevations are more complicated in these two
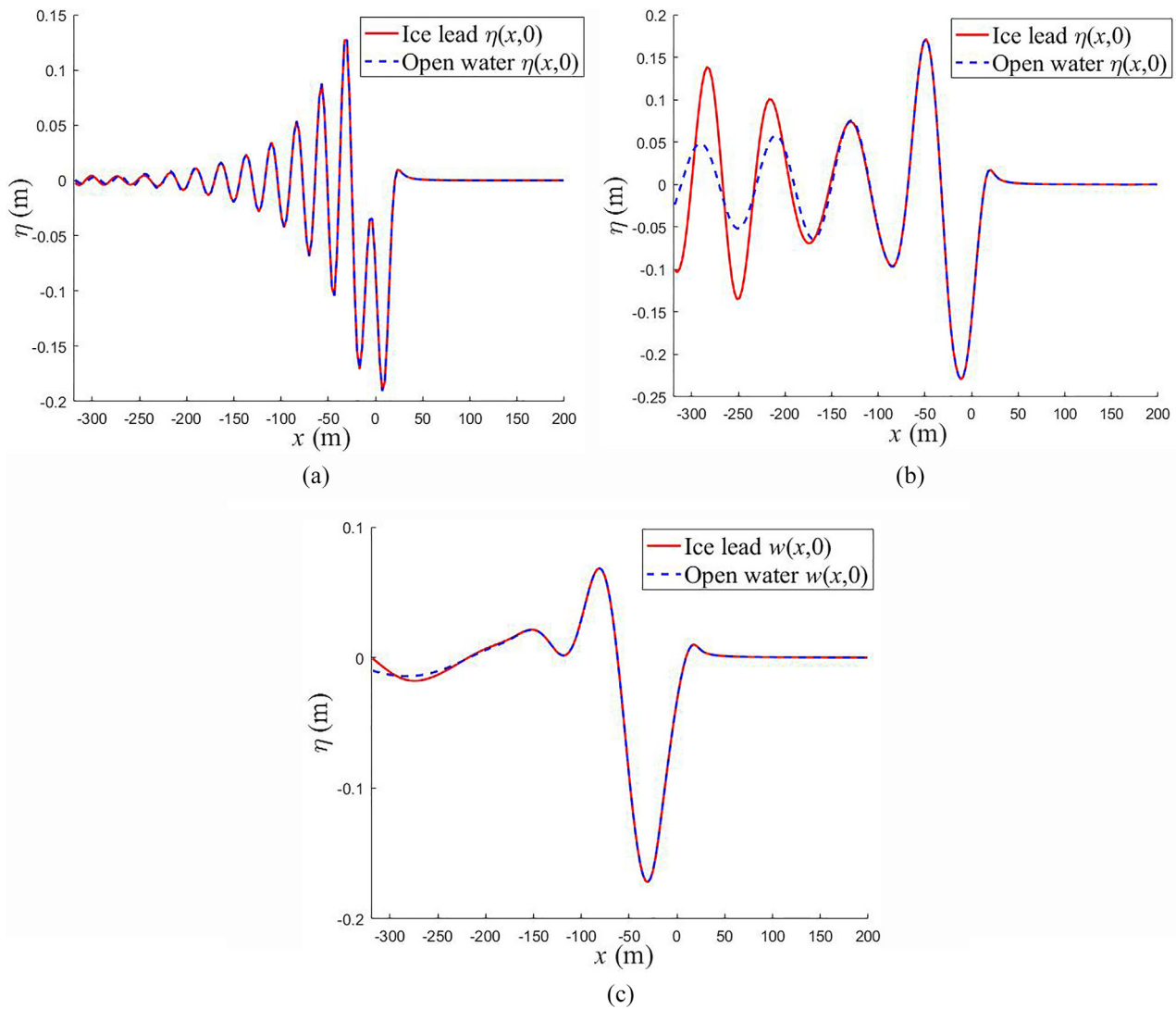

FIG. 15. The longitudinal profiles of water elevation along the central line, $y = 0$, of the channel for the load moving along the ice lead (solid lines) and on open water without ice (dashed lines): (a) subcritical case, $U = 6$ m/s; (b) critical case, $U_{cr}^{\infty} = 11.1$ m/s; and (c) supercritical case, $U = 20$ m/s.

cases. For critical case, the deflection of the ice sheet is confined to the region near the ice edge and behind the load. For supercritical speed, the deflection of the ice sheet propagates within a certain angle behind the load. Note that the wavelength becomes larger with increase in the speed. To show the details of ice deflections and free-surface elevations in these three cases, transverse and longitudinal profiles of ice sheets and the water surface in the lead are presented in Figs.15 and 16.

Figure 15 depicts the longitudinal profiles of water surface along the central line $y = 0$ for different speeds of the moving load. For comparison, the profiles without the presence of ice for the same load and the same parameters are shown by the dashed lines in the figure. For subcritical case, see Fig. 15(a), these two profiles almost coincide even far away from the load. The oscillation of the water surface is relatively regular, with the lowest depression under the load, the highest

elevation a short distance behind the load, and waves of decaying amplitude behind the load. Note that the free-surface elevation and the ice deflections are stationary in the system moving together with the load. The relaxation time, $\tau = 0.7$ s, in present calculations, is large, which explains the quick decay of the waves behind the load. In the critical case, see Fig. 15(b), the wave profile in the lead is different from that in completely open water but only in the wake behind the load. The waves in the lead behind the load decay slower than the waves on completely open water even for relatively large relaxation time. The waves in the lead behind the load are the superposition of the waves generated by the load and water waves reflected from the ice edges, which may result in the wave amplification behind the load. For the supercritical case, see Fig. 15(c), the free-surface elevation in the lead weakly depends on the presence of ice.
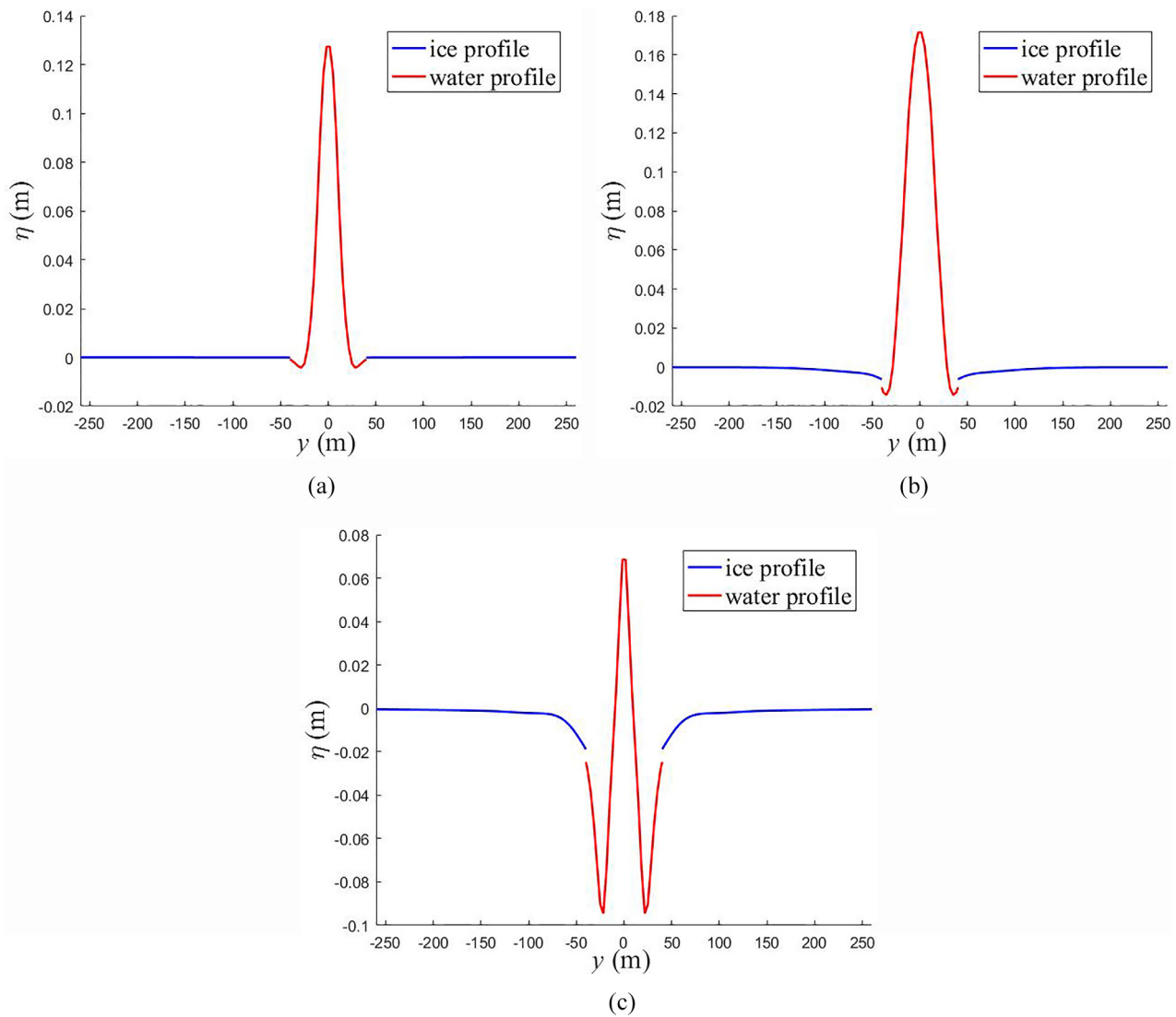

FIG. 16. The transverse profiles of both the water surface and ice surface through the highest water wave crests of Fig. 15. (a) subcritical case, $U = 6$ m/s; (b) critical case, $U_{cr}^{\infty} = 11.1$ m/s; and (c) supercritical case, $U = 20$ m/s.

Figure 16 provides the transverse profiles through the highest water wave crests of Fig. 15, which are approximately at $x = 30$ m, 49 m, and 81 m corresponding to subcritical case, critical case, and supercritical case. One can find that the deflection of ice sheet becomes larger as the speed increases. For subcritical case, deflection of the ice sheet is very small. For critical and supercritical cases, the ice deflections are maximum at the ice edge and decays with the distance from the edge without visible oscillations.

Figure 17 shows the deflection of the ice sheet and water elevation along the ice edge at $y = W/2$. Water elevation is usually higher than the deflection of ice edge. The wavelengths of the waves on both the ice sheet and water surface become longer, and the difference between the amplitude of the ice deflection and the water elevation decreases with increase in the load speed. For the subcritical case, only a very small localized deflection of the ice sheet occurs near the place of the load, see Fig. 17(a). For the critical and supercritical cases, waves in ice are formed visibly behind the load; see Figs. 17(b) and 17(c). The ice deflections in front of the load are restrained due to the large relaxation time (Shishmarev *et al.*, 2016).

The moving load generates waves on the water surface and in the ice. The flexural-gravity waves may break the ice plate. We restrict ourselves to the stress $\sigma_{xx}(x, W/2)$ along the ice edge. The stress
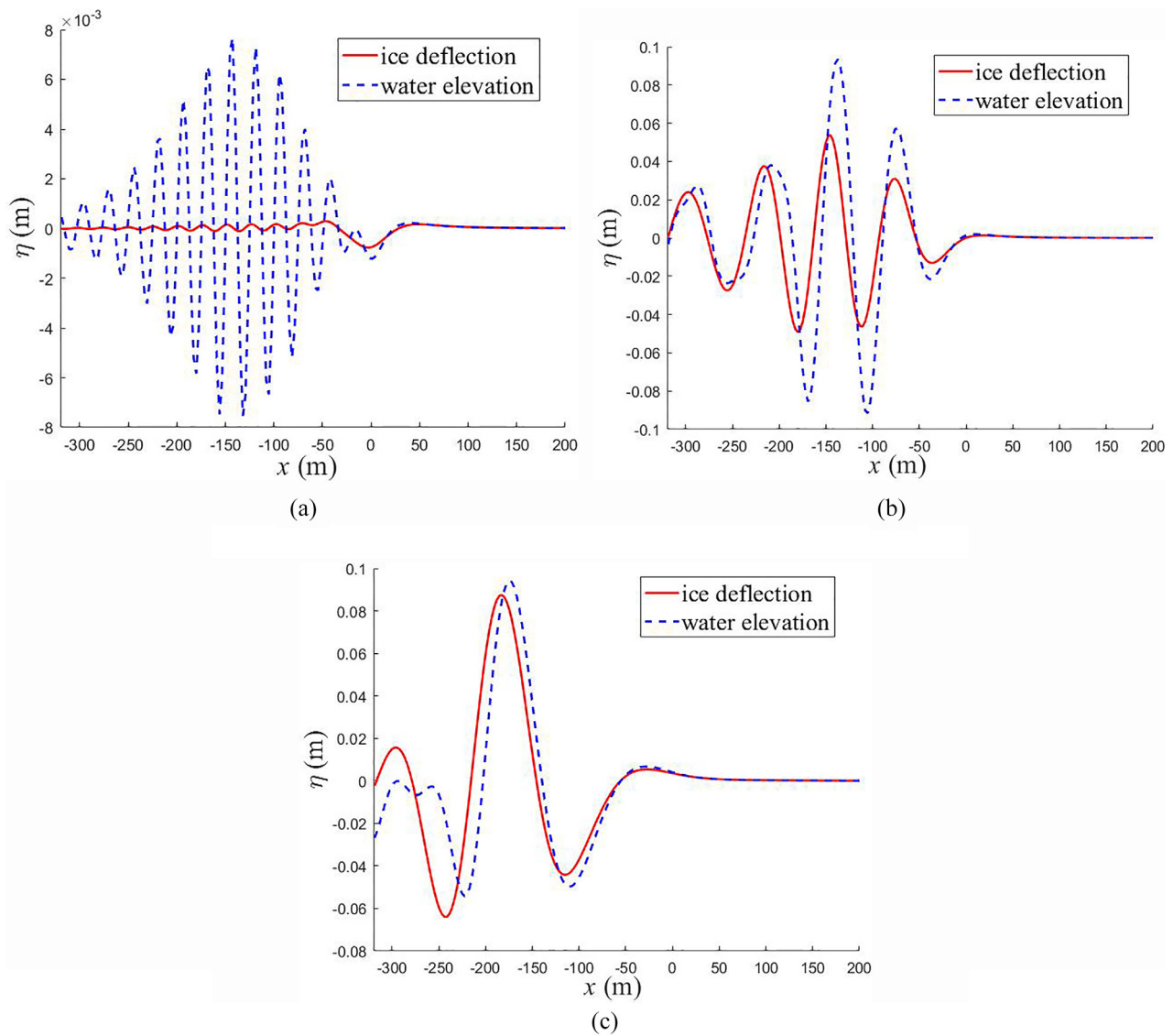

FIG. 17. The deflection of the ice sheet and water elevation along the ice edge at $y = W/2$: (a) Subcritical case, $U = 6$ m/s; (b) critical case, $U_{cr}^{\infty} = 11.1$ m/s; and (c) supercritical case, $U = 20$ m/s.
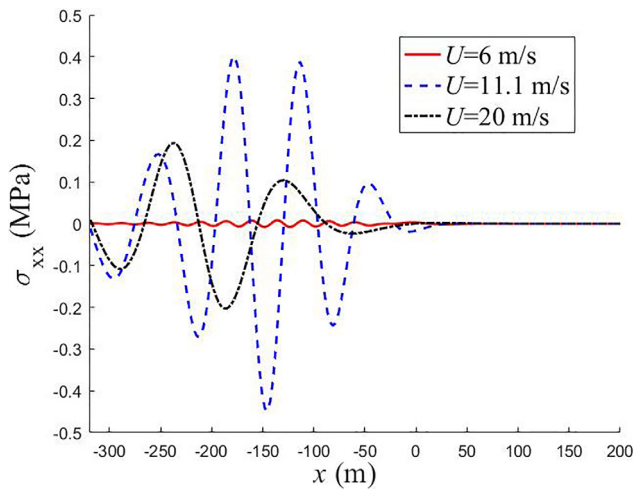
FIG. 18. The stress along the edge of ice sheet at $y = W/2$ for different speeds.

$\sigma_{yy}(x, W/2)$ is zero at the edge; see conditions (3). The formula (11) for the stress components and condition (3) provide $\sigma_{xx}(x, W/2) = \frac{Eh}{2}\left(1 - \tau U \frac{\partial}{\partial x}\right)\frac{\partial^2 \eta}{\partial x^2}$. The stress $\sigma_{xy}(x, W/2)$ is not zero at the ice edge but we do not consider this stress in the present study. The stress component $\sigma_{xx}(x, W/2)$ as a function of x is shown in Fig. 18 for three speeds of the load. The figure shows that the stress at $U = 6\,\text{m/s}$ is the lowest, which corresponds to the small deflection of ice edge at this subcritical speed, see Fig. 17. The maximum stress of ice edge at $U_{cr}^{\infty} = 11.1\,\text{m/s}$ is larger than that at $U = 20\,\text{m/s}$ although the maximum ice deflection is higher at $U = 20\,\text{m/s}$, as shown in Fig. 17. When the stress is larger than a failure stress of the ice sheet, cracks at the ice edge might be generated under the effects of a moving load. Within a linear model of ice plate deflection, the stresses near the ice edge are proportional to the magnitude of the load. Thus, one can

predict the required nominal pressure P_0 to break ice, provided the failure stress of the ice sheet is given.

B. Load speeds on maximum deflection and maximum stress

In this section, we investigate the maximum magnitude of the ice deflection, $\eta_{\max}(U) = \max_{-\infty<x<\infty}|\eta(x, W/2)|$, and the maximum magnitude of the bending stress, $\sigma_{\max}(U) = \max_{-\infty<x<\infty}|\sigma_{xx}(x, W/2)|$, along the edge of the ice plate as functions of the load speed U. Calculations were performed for the load speeds from 4 to 27 m/s. The maximum deflection, $\eta_{\max}(U)$, and maximum stress, $\sigma_{\max}(U)$, are shown on Fig. 19.

It is seen that both the maximum deflection, $\eta_{\max}(U)$, and the maximum stress, $\sigma_{\max}(U)$, at the ice edge are small for speeds below 6 m/s. Then both $\eta_{\max}(U)$ and $\sigma_{\max}(U)$ increase sharply. The maximum deflection of the edge, $\eta_{\max}(U)$, peaks at the load speed $U_{md} = 14.8\,\text{m/s}$, and the maximum stress, $\sigma_{\max}(U)$, peaks at the speed $U_{ms} = 11.85\,\text{m/s}$. Both load speeds, U_{md} and U_{ms}, are larger than the critical speed of the infinite elastic ice sheet, $U_{cr}^{\infty} = 11.1\,\text{m/s}$. As the load speed continues to increase, both the maximum deflection and maximum stress decay, see Fig. 19. Different from U_{cr}^{∞}, which is given by an analytical formula without account for the relaxation time τ, the speeds U_{md} and U_{ms} are obtained numerically for a given τ, given load and given parameters of the ice sheet and the lead. It is expected that for $\tau \to 0$ the speeds U_{md} and U_{ms} converge to a single speed U_{cr}^{lead}, and the peaks in Fig. 19 grow beyond all bounds. Note that U_{cr}^{lead} is expected to be different from U_{cr}^{∞}.

In the previous section, the critical speed of the infinite ice sheet, U_{cr}^{∞}, was chosen as a reference speed. However, Fig. 19 shows that $\eta_{\max}(U_{cr}^{\infty}) = 0.0538\,\text{m}$, which is approximately twice smaller than the maximum $\eta_{\max}(U_{md}) = 0.0982\,\text{m}$. Moreover, $\eta_{\max}(U) > \eta_{\max}(U_{cr}^{\infty})$ for load speeds from $U_{cr}^{\infty} = 11.1\,\text{m/s}$ up to $U = 27\,\text{m/s}$. Similarly, in the interval $U_{cr}^{\infty} < U < 14\,\text{m/s}$, Fig. 19(b) shows that $\sigma_{\max}(U)$ is greater than $\sigma_{\max}(U_{cr}^{\infty})$. Therefore, the critical speed for infinite ice
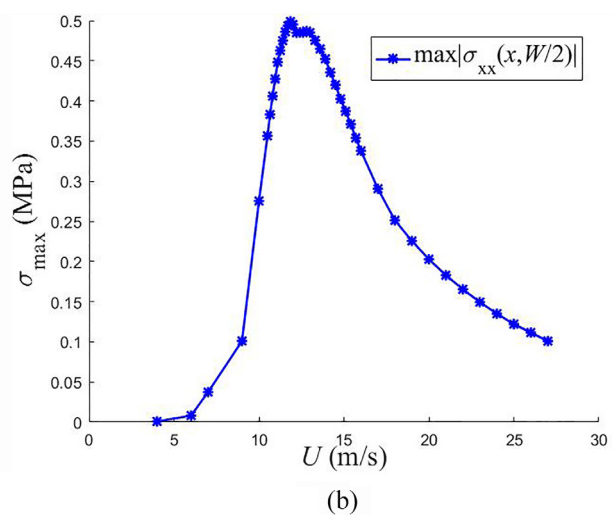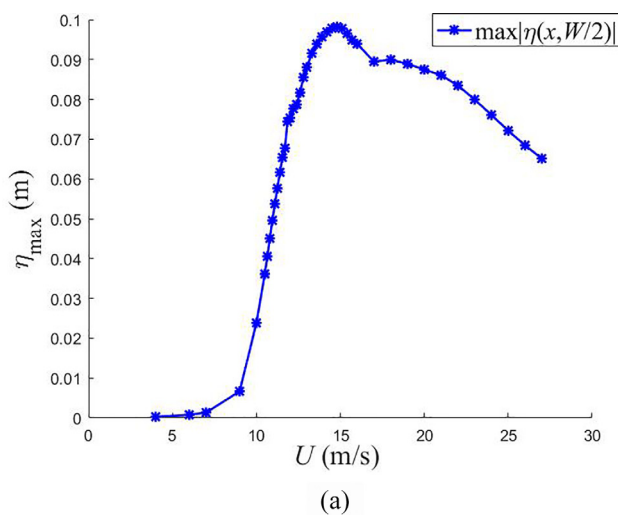

(a)

(b)

FIG. 19. (a) Maximum deflection, $\eta_{\max}(U)$, and (b) maximum stress, $\sigma_{\max}(U)$, along the ice edge.

sheet, in general, cannot be regarded as the critical speed of a load moving along the lead.

To illustrate difference between the ice response for U_{cr}^∞ and a speed U^* from the interval $U_{ms} < U^* < U_{md}$, we select $U^* = 13$ m/s and compare deflections and stresses calculated for speeds U_{cr}^∞ and $U^* = 13$ m/s. Figure 20 shows the deflection of the ice sheet along the edge, the bending stress components along the edge, and the longitudinal profiles of water elevation along the central line. One can see that both the magnitudes of both the ice deflections and stresses along the ice edge for $U^* = 13$ m/s are larger than those for U_{cr}^∞. Therefore, the critical speed for the infinite ice sheet cannot be regarded as the critical speed of a load moving in the ice lead. Figure 21 shows three-dimensional free surface elevation and ice deflection for speed $U^* = 13$ m/s. It is seen that the ice deflections for this speed are

higher than for U_{cr}^∞, see Fig. 14(b), can be observed at larger distances from the ice edge, and occur also in front of the load, compare with Fig. 14(c).

The difference of the speeds U_{md} and U_{ms} from U_{cr}^∞ can be explained by different geometries of the corresponding problems: U_{md} and U_{ms} are calculated for the ice sheet with a lead but U_{cr}^∞ is defined for the infinite ice sheet, as well as by the effect of the damping: U_{md} and U_{ms} are calculated with $\tau = 0.7$ s but U_{cr}^∞ is defined without account for damping. The effect of damping on the speeds U_{md} and U_{ms} can be understood calculating them for the infinite continuous ice sheet without a lead. The dashed lines in Figs. 28 and 29 depict $\eta_{\max}(U)$ and $\sigma_{\max}(U)$ for the infinite ice sheet without a crack, where $y = 0$ and $\tau = 0.7$ s, for the same conditions. It is seen that $\eta_{\max}(U)$ peaks at speed 12.2 m/s and $\sigma_{\max}(U)$ peaks at speed 11.85 m/s, both
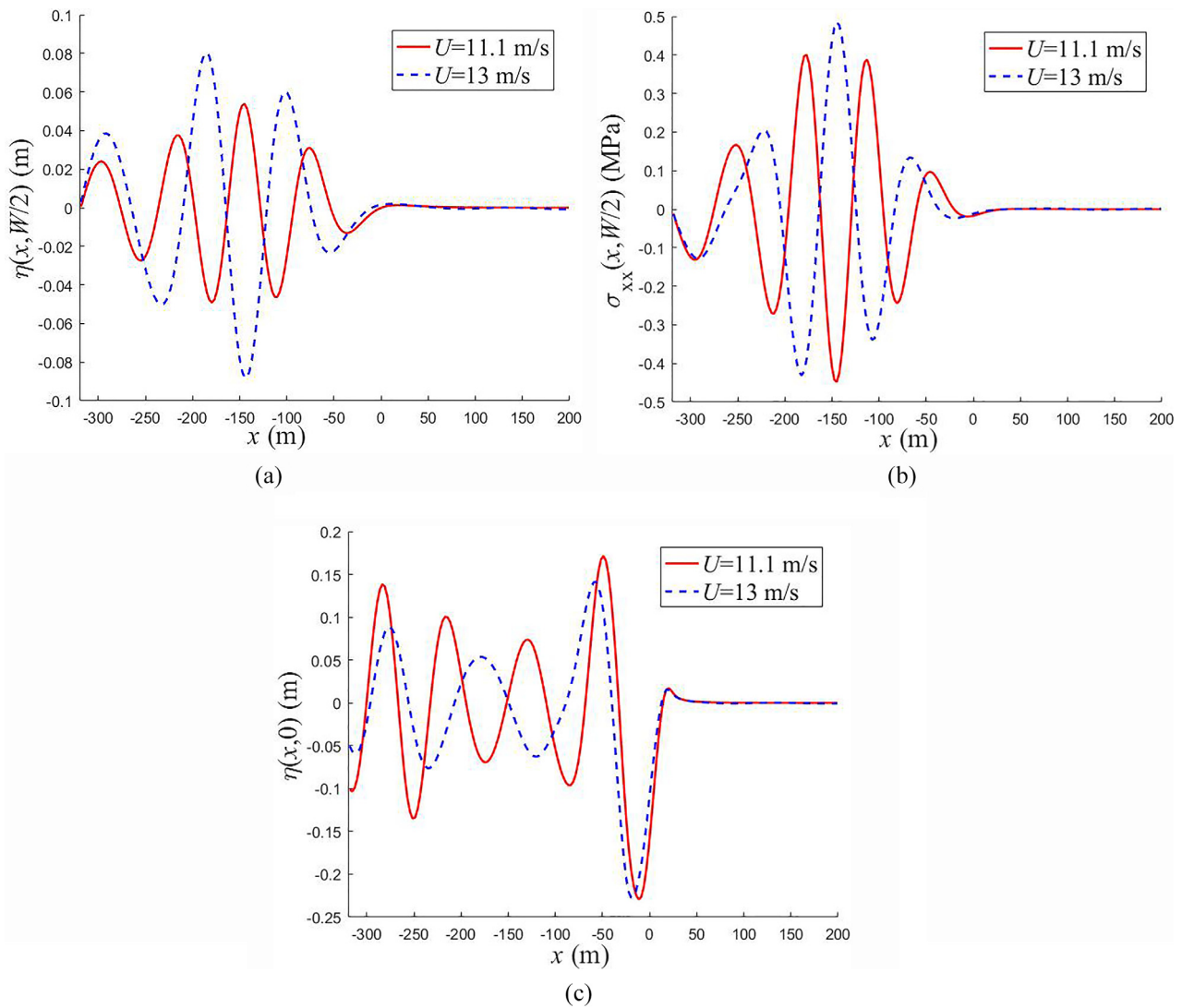

FIG. 20. (a) The ice deflection along the edge, (b) the stress along the edge, and (c) the longitudinal profile of water elevation along the centerline, $y = 0$, for $U_{cr}^\infty = 11.1$ m/s and $U^* = 13$ m/s.
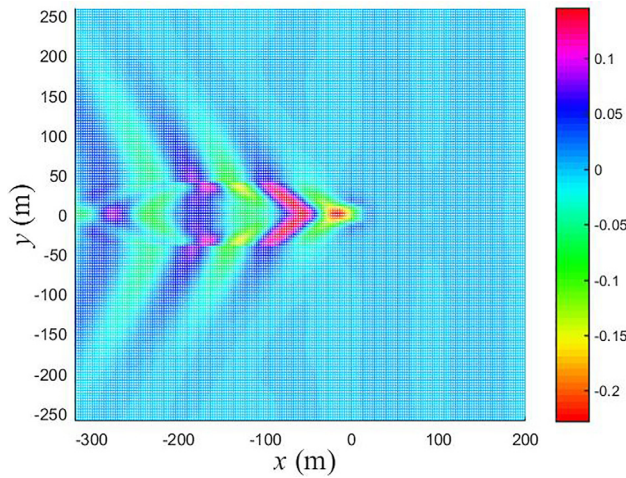
FIG. 21. Three-dimensional free surface elevation and ice deflection for speed 13 m/s.

of which are higher than the critical speed for the infinite ice sheet, U_{cr}^∞. Therefore, the relaxation time τ not only makes deflections and stresses finite for any speeds of the load, but also increase the speeds U_{md} and U_{ms} of maximum deflection and maximum stress.

C. Effect of the ice thickness

To investigate the effect of ice thickness on U_{md} and U_{ms}, the maximum ice deflection, $\eta_{\max}(U)$, and maximum stress, $\sigma_{\max}(U)$, along the ice edge are presented in Fig. 22 for $h = 0.4$ m and $h = 0.8$ m with the lead width $W = 2L = 80$ m and parameters of the load for case 4 from Table I. The corresponding critical speeds of infinite elastic ice sheet are 11.1 m/s for $h = 0.4$ m and 14.3 m/s for $h = 0.8$ m. It is seen that both speeds U_{md} and U_{ms} increase with increase in ice thickness. The speed $U_{md} = 21$ m/s for $h = 0.8$ m is much larger than the

corresponding critical speed of infinite elastic ice sheet. However, the speed $U_{ms} = 14.3$ m/s for $h = 0.8$ m is equal to the corresponding critical speed of infinite elastic ice sheet. Further research explaining the effects of ice elastic characteristics on stresses and deflections of the ice sheet is required. In particular, it would be interesting to know the speeds U_{md} and U_{ms} as functions of the ice thickness h.

D. Effect of the load properties

The ice response is proportional to the magnitude of the load within the linear model of hydroelasticity. The present calculations are done for $P_0 = 1000$ Pa, see Eq. (2). By using the obtained deflections and stresses, it is not complicated to find the ice response to any given load magnitude. Note that the total load is equal to $P_0 LB$ for any α and β in Eq. (2) for the load distribution. The maximum ice deflection, $\eta_{\max}(U)$, and maximum stress, $\sigma_{\max}(U)$, along the ice edge as functions of the load speed are presented in Fig. 23 for $\alpha = 5$, $\beta = 2.5$ and $\alpha = 10$, $\beta = 5$ with $W = 2L = 80$ m and $h = 0.4$ m. It is seen that both speeds U_{md} and U_{ms} weakly depend on α and β, but the magnitudes of both maximum ice deflection, $\eta_{\max}(U)$, and maximum stress, $\sigma_{\max}(U)$, increase with increase in α and β at a given load speed.

One may expect that the aspect-ratio of the load, L/B, where L is the length of the load along the lead and B is the width of the load, has an influence on the speed U_{md} and U_{ms}. The maximum ice deflection, $\eta_{\max}(U)$, and maximum stress, $\sigma_{\max}(U)$, along the ice edge as functions of the load speed are presented in Fig. 24 for different B and $L = 40$ m, $\alpha = 5$, $\beta = 2.5$, $h = 0.4$ m, $W = 80$ m. The total load $P_0 LB$ is constant in these calculations. The critical speed for infinite ice sheet for the same elastic characteristics of ice is $U_{cr}^\infty = 11.1$ m/s. The speed $U_{md} = 14.35$ m/s for $L/B = 1$, $U_{md} = 14.8$ m/s for $L/B = 2$, and $U_{md} = 15.1$ m/s for $L/B = 4$. The speed $U_{ms} = 11.85$ m/s for $L/B = 1$, $U_{ms} = 11.85$ m/s for $L/B = 2$, and $U_{ms} = 12.9$ m/s for $L/B = 4$. It is seen that both the speed U_{md} and U_{ms} increase with decrease in the width of the load across the lead. In other words, both speeds increase if the load becomes more elongated along the
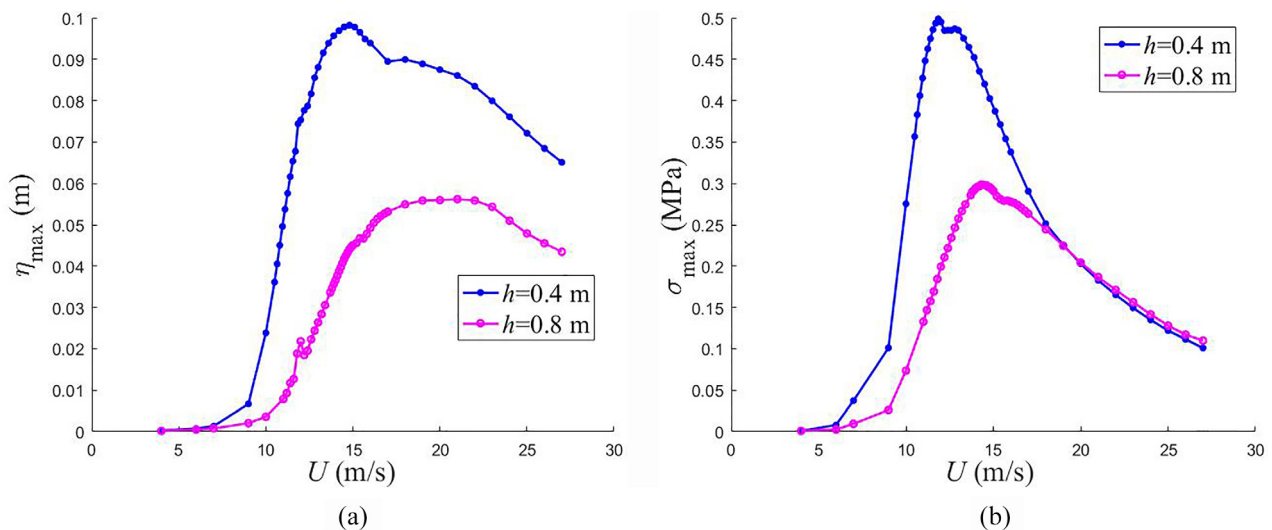

FIG. 22. (a) Maximum ice deflection, $\eta_{\max}(U)$, and (b) maximum stress, $\sigma_{\max}(U)$, along the ice edge, $y = W/2$, as functions of the load speed for $h = 0.4$ m and $h = 0.8$ m with $W = 2L = 80$ m and parameters of the load for case 4 from Table I.
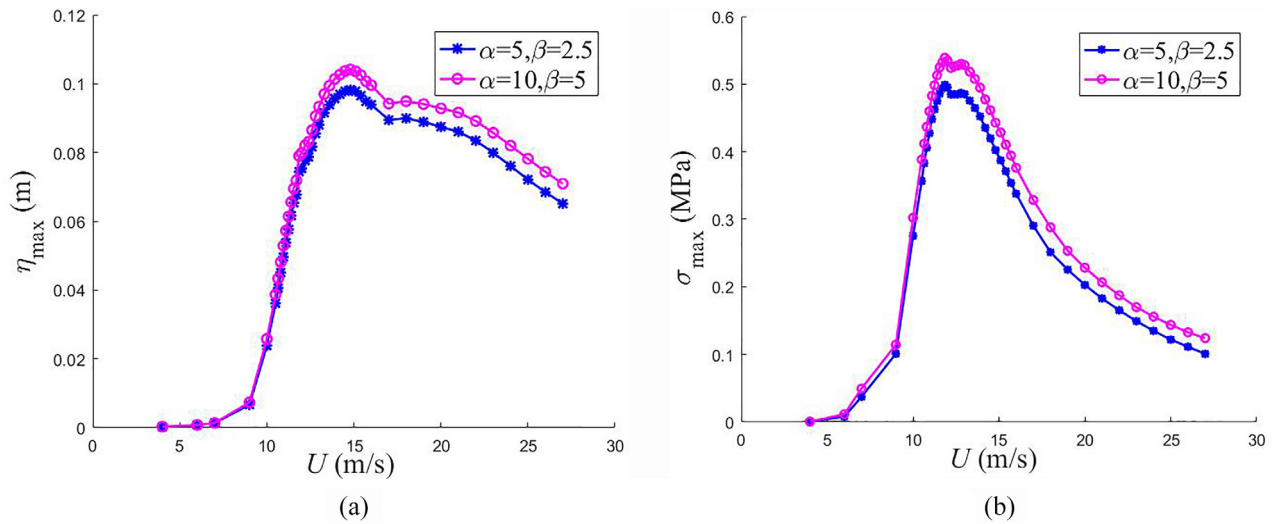
FIG. 23. (a) Maximum ice deflection, $\eta_{max}(U)$, and (b) maximum stress, $\sigma_{max}(U)$, along the ice edge, $y = W/2$, as functions of the load speed for $\alpha = 5$, $\beta = 2.5$ and $\alpha = 10$, $\beta = 5$ with $W = 2L = 80$ m and $h = 0.4$ m.

channel. All of these speeds are larger than the corresponding critical speed of infinite elastic ice sheet, $U_{cr}^{\infty} = 11.1$ m/s. It can be concluded that the larger the ratio L/B, the larger the ice deflection and stress in the ice sheet for a constant total load, $P_0 LB$. Further research clarifying the effect of load characteristics on ice response is required including the problems of non-uniform load and two loads moving at the same speed one after another.

E. Effect of the lead width

In terms of the effects of lead width on U_{md} and U_{ms}, the maximum ice deflections, $\eta_{max}(U)$, and maximum stresses, $\sigma_{max}(U)$, along the edge are presented in Fig. 25 for different lead widths with

$h = 0.4$ m and parameters of the load for case 4 from Table I. It is seen that U_{md} decreases as the lead width increases, but U_{ms} increases as the lead width increases. The speed $U_{md} = 14.8$ m/s for $W = 2L$ and $U_{md} = 14.5$ m/s for both $W = 3L$ and $4L$. The speed $U_{ms} = 11.85$ m/s for $W = 2L$, $U_{ms} = 12.2$ m/s for $W = 3L$, and $U_{ms} = 12.4$ m/s for $W = 4L$. Note that all of these speeds are larger than the corresponding critical speed of infinite elastic ice sheet, $U_{cr}^{\infty} = 11.1$ m/s. Further research on ice response for different widths of the lead is required with asymptotic analysis for very wide and very narrow leads. The meaning of wide lead with respect to the characteristic length of the ice sheet and dimensions of the load should be clarified.
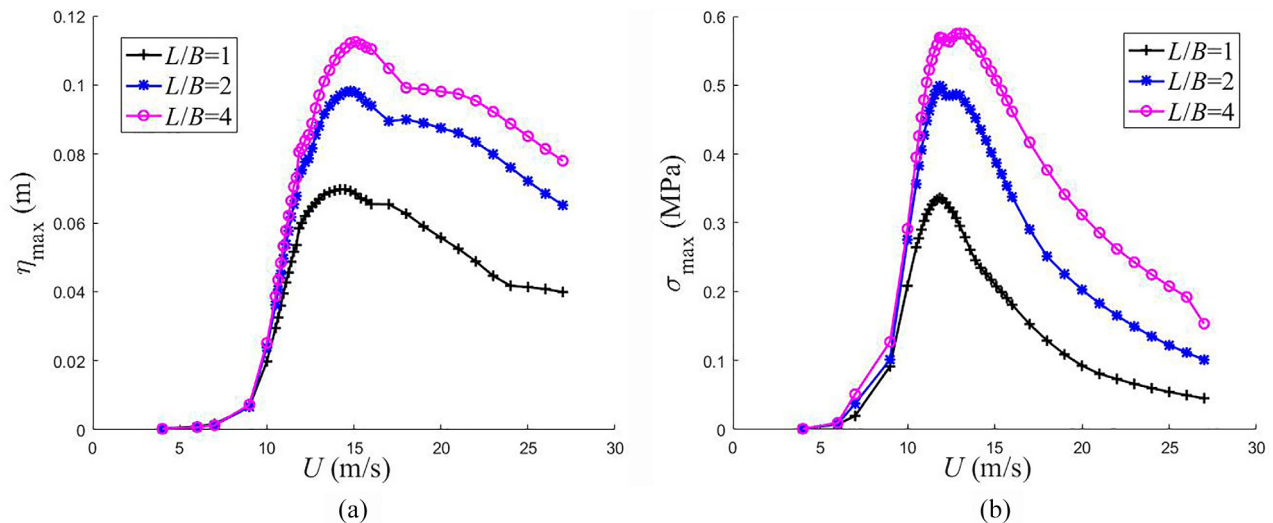

FIG. 24. (a) Maximum ice deflection, $\eta_{max}(U)$, and (b) maximum stress, $\sigma_{max}(U)$, along the ice edge, $y = W/2$, as functions of the load speed for different B and $L = 40$ m, $\alpha = 5$, $\beta = 2.5$, $h = 0.4$ m, $W = 80$ m. The total load $P_0 LB$ is constant.
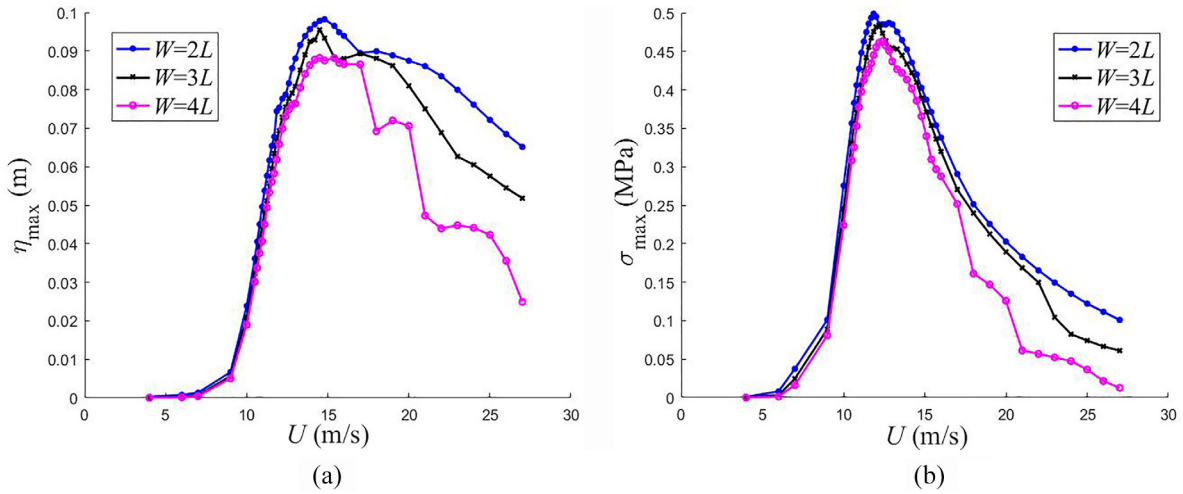
FIG. 25. (a) Maximum ice deflection, $\eta_{max}(U)$, and (b) maximum stress, $\sigma_{max}(U)$, along the ice edge, $y = W/2$, as functions of the load speed for different lead width with $h = 0.4$ m and parameters of the load for case 4 from Table I.
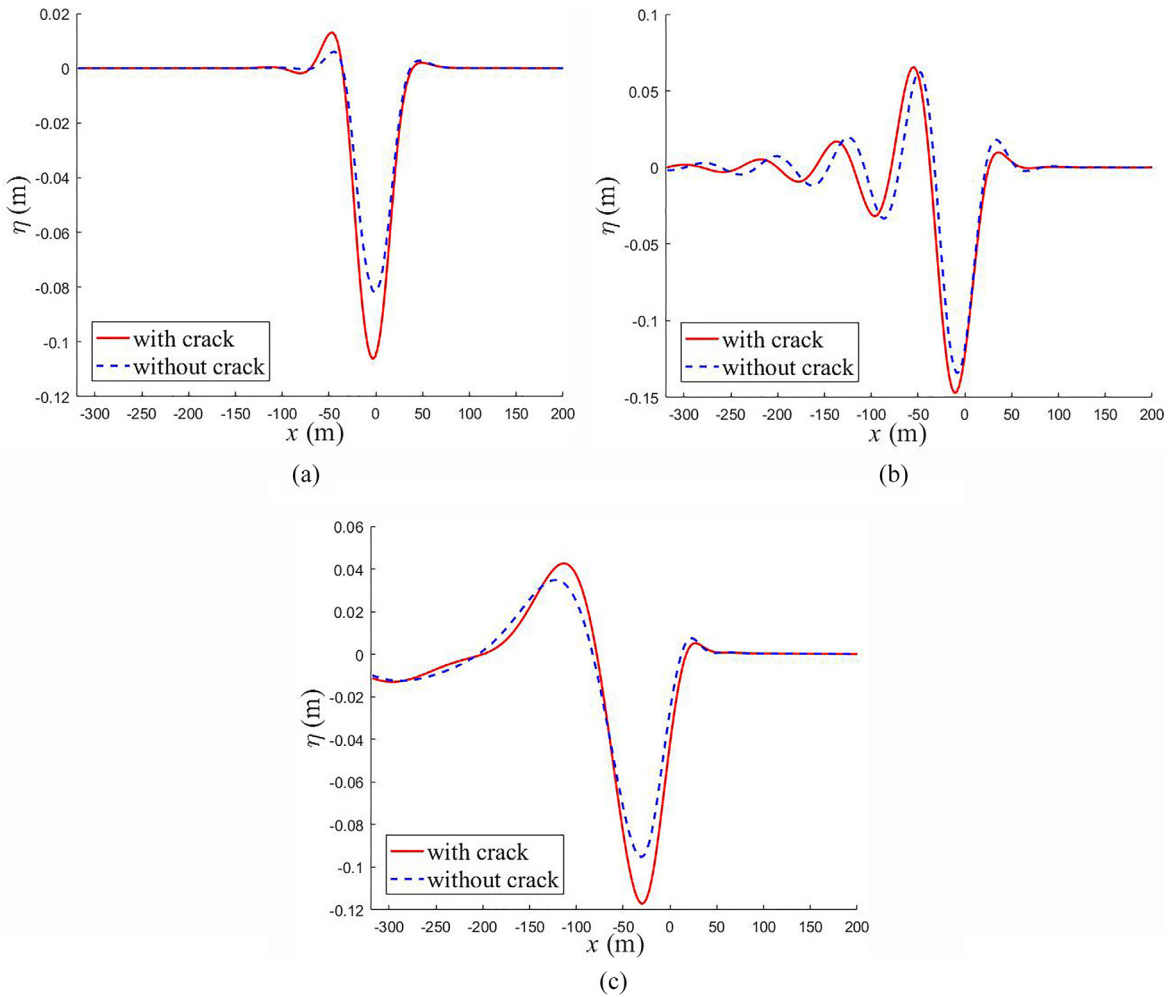

FIG. 26. Deflection of an infinite ice sheet along $y = 0$ with and without the crack: (a) subcritical case, $U = 6$ m/s; (b) critical case, $U_{cr}^{\infty} = 11.1$ m/s; and (c) supercritical case, $U = 20$ m/s.

VI. PRESSURE MOVING ON AN ICE SHEET ALONG A CRACK

If the bending stresses in the ice sheet are over the failure stress, cracks are generated in the ice sheet (Cui *et al.*, 2018; Yuan *et al.*, 2020), and the calculations should be terminated because generation and propagation of cracks are beyond the simulation ability of the present numerical model. However, the numerical algorithm can simulate the pressure moving on ice with an existing crack, which would be very helpful to understand the response of ice sheets after their damage. We consider a pressure moving on an infinite ice sheet with a crack at $y = 0$. The center of the pressure moves in the x direction along $y = 0$. The obtained results are compared with those for an infinite ice sheet without cracks.

Figure 26 provides the deflections $\eta(x, 0)$ of the ice sheet along $y = 0$ with and without the crack for three speeds of the load, $U = 6$, 11.1, and 20 m/s, where $U_{cr}^{\infty} = 11.1$ m/s is the critical speed for infinite continuous ice sheet. It is seen that the presence of the crack does not change significantly the ice deflections for any speed of the load. However, the deflections with the crack are slightly larger than without it.

Figure 27 provides the stress $\sigma_{xx}(x, 0)$ of the ice sheet along $y = 0$ with and without the crack for three speeds of the load, $U = 6$, 11.1, and 20 m/s. One can see that the stress $\sigma_{xx}(x, 0)$ oscillates both with and without crack. It is seen that the maximum stress of ice sheet without crack is larger than that of ice sheet without crack.

Figure 28 shows the maximum deflection, $\eta_{max}(U)$, of the ice sheet with and without crack as functions of the load speed U. The
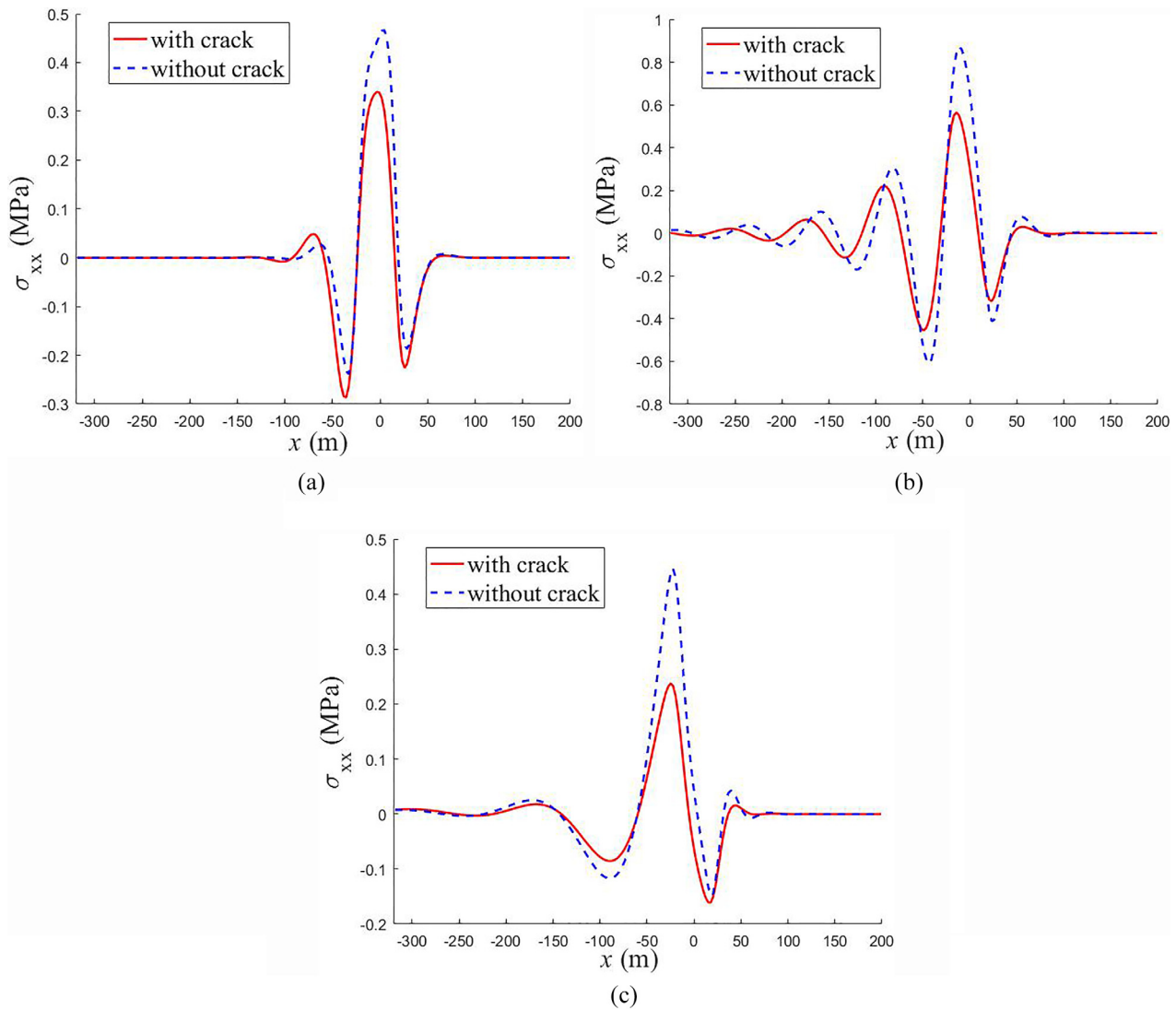

FIG. 27. Stress of an infinite ice sheet along $y = 0$ with and without the crack: (a) subcritical case, $U = 6$ m/s; (b) critical case, $U_{cr}^{\infty} = 11.1$ m/s; and (c) supercritical case, $U = 20$ m/s.
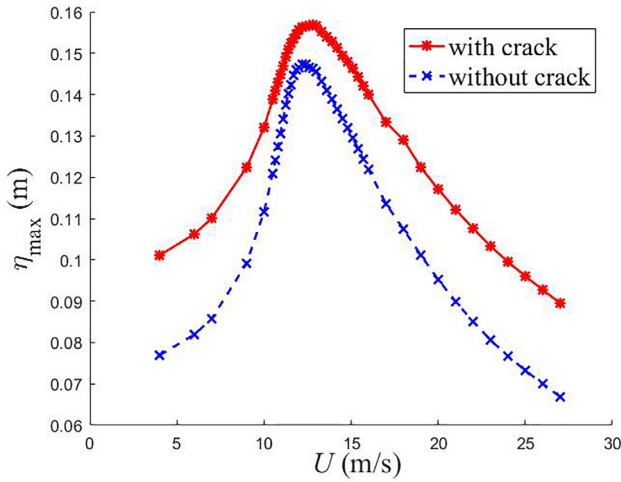
FIG. 28. The maximum deflection, $\eta_{max}(U)$, of an infinite ice sheet with and without crack.

FIG. 30. Resistance of pressure moving on an infinite ice sheet with and without a crack.

maximum deflection of infinite ice sheet with crack is larger than that of the intact ice sheet at each speed. For the ice sheet without and with crack, deflection magnitude peaks at $U_{md} \approx 12.2\,\mathrm{m/s}$ and $U_{md} \approx 12.8\,\mathrm{m/s}$, respectively. Both these speeds are higher than the critical speed of an infinite elastic plate, $U_{cr}^{\infty} = 11.1\,\mathrm{m/s}$. For the ice without the crack, this shift of the critical speed can be explained by the damping within the present viscoelastic model of ice sheet. For the ice with the crack, the shift in the critical speed is affected also by the presence of the crack in addition to the damping effect.

In contrast to the ice deflection, the maximum stress, $\sigma_{max}(U)$, of the infinite ice sheet with the crack is smaller than that of the intact ice sheet at each speed, as shown in Fig. 29. This also indicates that an ice sheet with an initial crack is hard to break again with the same load.
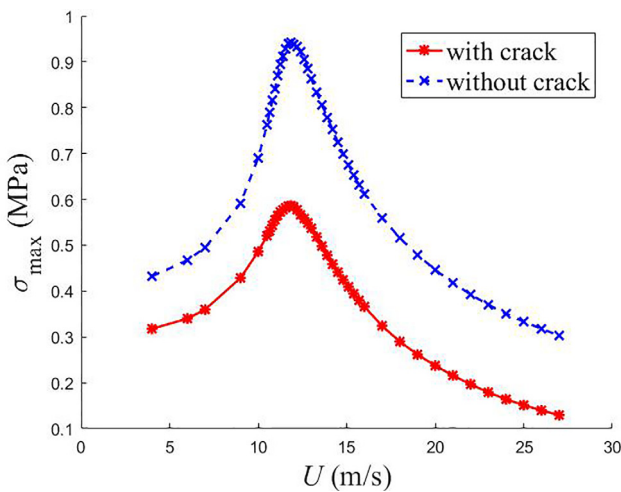
Whether the ice sheet is with or without crack, the stress peaks at $U_{ms} \approx 11.85\,\mathrm{m/s}$.

According to Eq. (9), the wave-making resistance of a moving load depends on the ice slope in the direction of the load motion. The resistances of the same load moving on ice sheet with and without crack are shown in Fig. 30. One can see that the resistance peaks at load speed $U_{mr} = 13.3\,\mathrm{m/s}$ for ice sheet with crack and 13 m/s for ice sheet without crack. We conclude that the wave-making resistance for the ice sheet with crack is slightly lower than that for the ice sheet without crack for load speeds close to U_{mr}.

VII. DISCUSSION AND CONCLUSION

A numerical method based on BIM has been proposed to estimate responses of ice sheets with a lead between them to a load moving on either ice or water surface. The method can deal with different conditions at the ice edge but it is limited to constant speed of the load and constant width of the lead. The approach allows variation of ice properties in the y-direction, perpendicular to the ice edge, but not in the x-direction along the ice edge. By introducing fictitious points along the ice edge within a finite difference method, the edge conditions were properly approximated. The approach and the numerical algorithm were validated by comparing the obtained results to the results obtained by different methods.

For the pressure moving in an ice lead, elevation of the water surface and the deflection of the ice sheet oscillate for the load speeds being close to the critical speed U_{cr}^{∞}. Interaction of the waves generated by the moving load and reflected by the ice edges amplifies the water waves behind the load for critical and supercritical speeds of the load. This wave amplification is likely to influence a body moving behind the load, like a merchant ship following an ice-breaker. For case 4 from Table I, the maximum deflection of ice sheet peaks at $U_{md} \approx 14.8\,\mathrm{m/s}$, while the maximum stress of ice sheet peaks at $U_{ms} \approx 11.85\,\mathrm{m/s}$. We concluded that both the wave amplitude and the wavelength contribute to the stress magnitude, which explains the difference between U_{ms} and U_{md}. Both of them are higher than the critical speed of infinite elastic plate, $U_{cr}^{\infty} = 11.1\,\mathrm{m/s}$, under the

FIG. 29. The maximum stress, $\sigma_{max}(U)$, of an infinite ice sheet with and without crack.

combined effects of boundary conditions and damping of the ice sheets. The speeds U_{md} and U_{ms} increase with increase in ice thickness. As the lead width increase, the speed U_{md} decreases but the speed U_{ms} increases. Variation of the parameters α and β in Eq. (2) does not change significantly the speeds U_{md} and U_{ms}, but they increase with increase in the ratio L/B. The larger the ratio L/B, the larger the ice deflection and stress in the ice sheet for a constant total load, P_0LB.

For the pressure moving on an infinite ice sheet with a crack, the results were compared with those for the pressure moving on an infinite ice without the crack. The maximum deflection of ice sheet with a crack is always larger than for the ice sheet without a crack. The deflection peaks at the load speed $U_{md} = 12.8\,\text{m/s}$ for the ice sheet with the crack and at $U_{md} \approx 12.2\,\text{m/s}$ for the ice sheet without a crack. Therefore, the presence of a crack makes the ice sheet easier to deform under the same pressure load. In contrast, the maximum stress in the ice sheet with a crack is always lower than in the ice sheet without a crack although the peaks of the maximum stress for these two cases reach at the same speed, $U_{ms} = 11.85\,\text{m/s}$. This indicates that the existence of initial crack makes the ice sheet more difficult to break by using the same moving pressure. With respect to the wave-making resistance, it is slightly lower for a moving on an ice sheet with a crack than that for the same load moving on an intact ice sheet and only for load speeds close to the speed of maximum resistance U_{mr}. Last but not least, one should notice that the difference in the numerical results between the ice sheets with and without a crack comes only from the free-edge boundary conditions. In other words, if the free-edge boundary conditions are not incorporated properly in the numerical model, then the numerical results will be inconsistent.

AUTHORS' CONTRIBUTIONS

All authors contributed equally to this work.

ACKNOWLEDGMENTS

DATA AVAILABILITY

The data that support the findings of this study are available from the corresponding author upon reasonable request.

REFERENCES

Batyaev, E. A., and Khabakhpasheva, T. I. "Hydroelastic waves in a channel covered with a free ice sheet," Fluid Dyn. **50**(6), 775–788 (2015).

Bonnefoy, F., Meylan, M. H., and Ferrant, P., "Nonlinear higher order spectral solution for a two-dimensional moving load on ice," J. Fluid Mech. **621**, 215–242 (2009).

Brocklehurst, P., "Hydroelastic waves and their interaction with fixed structures," Ph.D. thesis (University of East Anglia, 2012).

Chung, H., and Linton, C. M., "Reflection and transmission of waves across a gap between two semi-infinite elastic plates on water," Q. J. Mech. Appl. Math. **58**(1), 1–15 (2005).

Cui, P., Zhang, A. M., Wang, S. P., and Khoo, B. C., "Ice breaking by a collapsing bubble," J. Fluid Mech. **841**, 287–309 (2018).

Davys, J. W., Hosking, R. J., and Sneyd, A. D., "Waves due to a steadily moving source on a floating ice plate," J. Fluid Mech. **158**(1), 269 (1985).

Dinvay, E., Kalisch, H., and Parau, E. I., "Fully dispersive models for moving loads on ice sheets," J. Fluid Mech. **876**, 122–149 (2019).

Doctors, L. J., and Sharma, S. M., "The wave resistance of an air-cushion vehicle in steady and accelerated motion," J. Ship Res. **16**(4), 248–260 (1972).

Ertekin, R. C., and Xia, D. W., "Hydroelastic response of a floating runway to cnoidal waves," Phys. Fluids **26**(2), 027101 (2014).

Evans, D. V., and Porter, R., "Wave scattering by narrow cracks in ice sheets floating on water of finite depth," J. Fluid Mech. **484**, 143–165 (2003).

Hess, J. L., and Smith, A. M. O., "Calculation of nonlifting potential flow about arbitrary three dimensional bodies," J. Ship Res. **8**(2), 22–44 (1964).

Hosking, R. J., Sneyd, A. D., and Waugh, D. W., "Viscoelastic response of a floating ice plate to a steadily moving load," J. Fluid Mech. **196**(1), 409–430 (1988).

Khabakhpasheva, T. I., Shishmarev, K., and Korobkin, A. A., "Large-time response of ice cover to a load moving along a frozen channel," Appl. Ocean Res. **86**, 154–165 (2019).

Kheisin, D. Y., "Moving load on an elastic plate which floats on the surface of an ideal fluid (in Russian)," Ivz. AN SSSR, Otd, Tekh. i Mashinstroenie **1**, 178–180 (1963).

Korobkin, A. A., Khabakhpasheva, T. I., and Papin, A. A., "Waves propagating along a channel with ice cover," Eur. J. Mech. B **47**, 166–175 (2014).

Kozin, V. M., and Pogorelova, A. V., "Wave resistance of amphibian aircushion vehicles during motion on ice fields," J. Appl. Mech. Tech. Phys. **44**(2), 193–197 (2003).

Kozin, V. M., and Pogorelova, A. V., "Effect of the viscosity properties of ice on the deflection of an ice sheet subjected to a moving load," J. Appl. Mech. Tech. Phys. **50**(3), 484–492 (2009).

Letcher, J. S., "Properties of finite-difference operators for the steady-wave problem," J. Ship Res. **37**(1), 1–7 (1993).

Li, Y., Liu, J., Hu, M., and Zhang, Z., "Numerical modeling of ice-water system response based on rankine source method and finite difference method," Ocean Eng. **138**, 1–8 (2017).

Li, Z. F., Shi, Y. Y., and Wu, G. X., "Interaction of wave with a body floating on a wide polynya," Phys. Fluids **29**, 097104 (2017).

Li, Z. F., Shi, Y. Y., and Wu, G. X., "Interaction of waves with a body floating on polynya between two semi-infinite ice sheets," J. Fluids Struct. **78**, 86–108 (2018a).

Li, Z. F., Wu, G. X., and Ji, C. Y., "Wave radiation and diffraction by a circular cylinder submerged below an ice sheet with a crack," J. Fluid Mech. **845**, 682–712 (2018b).

Liu, J. B., Zhang, Z. H., Zhang, L. Y., and Yao, J., "Application of mixed BEM and FDM in numerical simulation of ice-breaking by air cushion vehicle (in Chinese)," J. Naval Univ. Eng. **25**(3), 50–55 (2013).

Marchenko, A. V., "Resonance interactions of waves in an ice channel," J. Appl. Mathematics Mech. **61**(6), 931–940 (1997).

Mase, G. E. *Theory and Problems of Continuum Mechanics* (McGraw-Hill, New York, 1970).

Milinazzo, F., Shinbrot, M., and Evans, N. W., "A mathematical analysis of the steady response of floating ice to the uniform motion of a rectangular load," J. Fluid Mech. **287**, 173–197 (1995).

Ni, B. Y., Han, D. F., Di, S. C., and Xue, Y. Z., "On the development of ice-water-structure interaction," J. Hydrodynamics **32**(4), 629–652 (2020).

Parau, E. I., and Dias, F., "Nonlinear effects in the response of a floating ice plate to a moving load," J. Fluid Mech. **460**, 281–305 (2002).

Parau, E. I., and Vanden-Broeck, J. M., "Three-dimensional waves beneath an ice sheet due to a steadily moving pressure," Philos. Trans. R. Soc. A **369**(1947), 2973–2988 (2011).

Parau, E. I., Vanden-Broeck, J. M., and Cooker, M. J., "Three-dimensional capillary-gravity waves generated by a moving disturbance," Phys. Fluids **19**(8), 082102 (2007).

Pogorelova, A. V., and Kozin, V. M., "Flexural-gravity waves due to unsteady motion of point source under a floating plate in fluid of finite depth," J. Hydrodynamics **22**(5-supp-S1), 71–76 (2010).

Porter, R., "Trapping of waves by thin floating ice floes," Quart. J. Mech. Appl. Math. **71**(4), 463–483 (2018).

Ren, K., Wu, G. X., and Thomas, G. A., "Wave excited motion of a body floating on water confined between two semi-infinite ice sheets," Phys. Fluids **28**(12), 127101 (2016).

Ren, K., Wu, G. X., and Li, Z. F., "Hydroelastic waves propagating in an ice-covered channel," J. Fluid Mech. **886**(A18), 1–24 (2020).

Raven, H., "A solution method for the nonlinear ship wave resistance problem," Ph.D. thesis (TU Delft, 1996).

Schulkes, R. M. S. M., and Sneyd, A. D., "Time-dependent response of floating ice to a steadily moving load," J. Fluid Mech. **186**(1), 25–46 (1988).

Shi, Y. Y., Li, Z. F., and Wu, G. X., "Interaction of wave with multiple wide polynyas," Phys. Fluids **31**, 042106 (2019).

Shishmarev, K., Khabakhpasheva, T. I., and Korobkin, A. A., "The response of ice cover to a load moving along a frozen channel," Appl. Ocean Res. **59**, 313–326 (2016).

Shishmarev, K., Khabakhpasheva, T. I., and Korobkin, A. A., "Ice response to an underwater body moving in a frozen channel," Appl. Ocean Res. **91**, 101877 (2019).

Squire, V. A., "Of ocean waves and sea-ice revisited," Cold Regions Sci. Technol. **49**(2), 110–133 (2007).

Squire, V. A., Hosking, R. J., Kerr, A. D., and Langhorne, P. J., *Moving Loads on Ice Plates* (Kluwer Academic Publishers, 1996).

Squire, V. A., Robinson, W. H., Haskell, T. G., and Moore, S. C., "Dynamic strain response of lake and sea ice to moving loads," Cold Regions Sci. Technol. **11**(2), 123–139 (1985).

Sturova, I. V., "Motion of an external load over a semi-infinite ice sheet in the subcritical regime," Fluid Dyn. **53**(1), 49–58 (2018).

Sturova, I. V., and Tkacheva, L. A., "The motion of pressure distribution over a free surface near the edge of ice sheet," IOP Conf. Ser. **193**(1), 012065 (2018).

Sturova, I. V., and Tkacheva, L. A., "Movement of external load over free surface of fluid in the ice channel," J. Phys.: Conf. Ser. **1268**, 012066 (2019).

Takizawa, T., "Deflection of a floating sea ice sheet induced by a moving load," Cold Regions Sci. Technol. **11**(2), 171–180 (1985).

Tkacheva, L. A., "Edge waves produced by the motion of a vessel in an ice channel," J. Appl. Mech. Tech. Phys. **60**(5), 850–864 (2019a).

Tkacheva, L. A., "Wave motion in an ice sheet with crack under uniformly moving Load," Fluid Dyn. **54**(1), 14–32 (2019b).

Yuan, G. Y., Ni, B. Y., Wu, Q. G., Xue, Y. Z., and Zhang, A. M., "An experimental study on the dynamics and damage capabilities of a bubble collapsing in the neighborhood of a floating ice cake," J. Fluids Struct. **92**, 102833 (2020).